ACS OMEGA

Open Access

http://pubs.acs.org/journal/acsodf

Article

Fumaria indica (Hausskn.) Pugsley Hydromethanolic Extract: Bioactive Compounds Identification, Hypotensive Mechanism, and Cardioprotective Potential Exploration

Syed Adil Hussain Shah, Samia Latif Rana, Mohamed Mohany, Marija Milošević, Salim S. Al-Rejaie, Muhammad Akmal Farooq, Muhammad Naeem Faisal, and Ambreen Aleem*

Cite This: *ACS Omega* 2024, 9, 3642−3668

Read Online

ACCESS | Metrics & More | Article Recommendations | Supporting Information

ABSTRACT: *Fumaria indica* (Hausskn.) Pugsley (FIP), a member of the Papaveraceae family, has a documented history of use in traditional medicine to treat cardiovascular ailments, particularly hypertension, and has shown substantial therapeutic efficacy among native cultures worldwide. However, the identification of bioactive compounds and the mechanism of hypotensive effect with the cardioprotective potential investigations are yet to be determined. The study aimed to identify bioactive compounds, explore the hypotensive mechanism and cardioprotective potential, and assess the safety of *Fumaria indica* (Hausskn.) Pugsley hydromethanolic extract (Fip.Cr). LC ESI-MS/MS analysis was performed to identify the bioactive compounds. In vitro experiments were conducted on isolated rat aorta and atria, and an *in vivo* invasive BP measurement model was used. Acute and subacute toxicities were assessed for 14 and 28 days, respectively. Isoproterenol (ISO) was used to develop the rats' myocardial infarction damage model. The mRNA levels of NLRP3 inflammasome and the abundance level of Firmicutes and Lactobacillus were measured by qRT-PCR. The hypotensive effect of FIP bioactive compounds was also investigated using in silico methods. Fip. Cr LC ESI−MS/MS analysis discovered 33 bioactive compounds, including alkaloids and flavonoids. In isolated rat aorta, Fip.Cr reversed contractions induced by K^+ (80 mM), demonstrating a calcium entry-blocking function, and had a vasorelaxant impact on phenylephrine (PE) (1 μM)-induced contractions unaffected by L-NAME, ruling out endothelial NO participation. Fip.Cr caused negative chronotropic and inotropic effects in isolated rat atria unaffected by atropine pretreatment, eliminating cardiac muscarinic receptor involvement. Safety evaluation showed no major adverse effects. In vivo, invasive BP measurement demonstrated a hypotensive effect comparable to verapamil. Fip.Cr protected the rats from ISO-induced MI interventions significantly in biometrical and cardiac serum biochemical indicators and histological examinations by reducing inflammation via inhibiting NLRP3 inflammasome and elevating Firmicutes and Lactobacillus levels. The network pharmacology study revealed that the FIP hypotensive mechanism might involve MMP9, JAK2, HMOX1, NOS2, NOS3, TEK, SERPINE1, CCL2, and VEGFA. The molecular docking study revealed that FIP bioactive compounds docked better with CAC1C_ HUMAN than verapamil. These findings demonstrated that Fip.Cr's hypotensive mechanism may include calcium channel blocker activity. Fip.Cr ameliorated ISO-induced myocardial infarction in rats by attenuating inflammation, which might be via inhibiting NLRP3 inflammasome and may prove beneficial for treating MI.

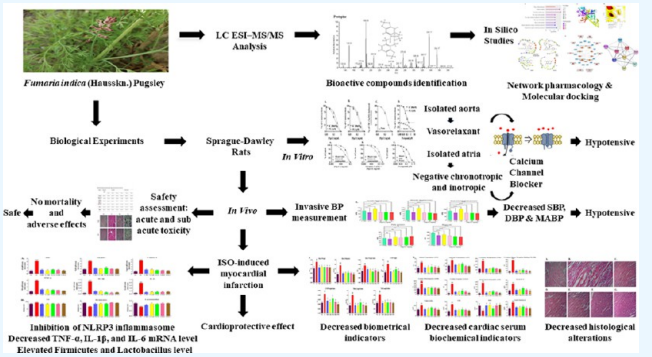

1. INTRODUCTION

Cardiovascular diseases (CVDs) are the leading cause of mortality and significantly detriment to life quality. CVDs include peripheral arterial and ischemic heart disease, heart failure, stroke, and other vascular and cardiac diseases.[1,2] In 2017, cardiovascular disease caused 17.8 million fatalities, life loss of 330 million years, and additional disability of 35.6 million.[3] According to the WHO, 17.5 million people die yearly from CVDs, representing 31% of all deaths globally.[4] Heart disease accounts for approximately 7.4 million annual deaths, whereas stroke is responsible for 6.7 million annual fatalities.[5,6] People with heart conditions may be more vulnerable to COVID-19 illness.[7,8]

Hypertension is a major cardiovascular disease risk factor. WHO has identified it as one of the most significant worldwide

Received: October 2, 2023
Revised: November 26, 2023
Accepted: December 11, 2023
Published: January 6, 2024

Table 1. Bioactive Compound Identification of *Fumaria indica* (Hausskn.) Pugsley Hydromethanolic Extract by LC ESI-MS/MS Analysis[a]

sr. no.	analysis mode	rt (min)	*m/z*	product ions (*m/z*)	accurate mass	identified compound	compound class	references
1	[M − H]−	0.44	160.90	162.17, 161, 133	162.0317	umbelliferone	coumarins and derivatives	MassBank BS003401
2	[M − H]−	0.53	162.90	162.92, 134.92, 119, 116.92	164.04734	2-coumaric acid	coumarins and derivatives	MassBank KO000443
3	[M − H]−	1.40	177.20	177.17, 149, 133, 105.17	178.02661	daphnetin	coumarins	MassBank PR100936
4	[M − H]−	1.69	191.00	191, 177.33, 176, 149.92, 148.92	192.04226	scopoletin	coumarins	MassBank FIO00954
5	[M − H]−	2.29	223.22	223, 209.17, 179, 165.08, 149.08, 147.08	224.06847	sinapic acid	hydroxycinnamic acids	MassBank PR307062
6	[M − H]−	3.05	279.20	279.25, 261.17, 259.17, 243.25, 233.17, 215.92, 205.17	280.24023	linoleic acid	fatty Acyls	MassBank MT000114
7	[M − H]−	8.08	293.20	293.17, 275.25	294.398	koumidine	alkaloids	MassBank PR308858
8	[M − H]−	8.72	313.20	295.25, 269.08, 233.25, 213.17, 183.17, 171.17, 121	314.079038	3,7-dihydroxy-3′,4′-dimethoxyflavone	flavonoids	MassBank BML01698
9	[M − H]−	9.35	327.30	327, 312.25, 291.17, 221.08, 209, 165.17	328.273	bergenin	gallic acid and derivatives	MassBank PR307403
10	[M − H]−	12.22	420.50	420, 394.33, 357.17, 340.25,	421.509	(methylsulfanyl) butyl glucosinolate	glucosinolates	MassBank PR309205
11	[M − H]−	12.46	427.30	427.25, 412.08, 383.25	428.485	isomajdine	alkaloids	MassBank PR304792
12	[M + H]+	0.26	149.00	149.08, 122.92, 121, 119, 103, 93.08, 91.08	148.161	p-coumaraldehyde	cinnamic acid and derivatives	MassBank PR310503
13	[M + H]+	0.32	165.00	137, 135.08, 133, 125.08, 109.08, 107.08, 105	164.08373	eugenol	phenylpropanoid	MassBank FIO00504
14	[M + H]+	0.67	177.00	177.08, 149, 145, 135	176.09496	serotonin	amino compound	MassBank KO004017
15	[M + H]+	2.17	193.00	193.08, 181, 178.08, 175.08, 165.08, 151.08	192.04226	scopoletin	coumarins	MassBank PB002204
16	[M + H]+	3.09	206.00	206.08, 191.08, 188.08, 175, 163, 149	205.257	dehydrosalsolidine	dihydroisoquinolines	MassBank PR301442
17	[M + H]+	3.19	207.00	207, 192.08, 179.08, 175, 150	206.197	scoparone	coumarins and derivatives	MassBank PR303602
18	[M + H]+	3.20	222.20	222, 207.17, 189.08, 179.17, 177.08, 166.25, 165.08, 162.92	221.256	hydrocotarnine	tetrahydroisoquinolines	MassBank PR300973
19	[M + H]+	3.42	247.20	247.08, 229.08, 219.08, 217.08, 205.08, 191, 189.08	246.313	ellipticine	carbazoles	MassBank PR301242
20	[M + H]+	4.20	265.20	265.08, 237.08, 219.08, 205, 191.08, 179.08	264.13617	hulupinic acid	terpenoids	MassBank FIO01070
21	[M + H]+	4.93	283.20	268.08, 253.08, 251.08, 237.08, 225.08, 197.08	282.089209	2′,5-dimethoxyflavone	flavone	MassBank BML01779
22	[M + H]+	5.80	307.20	307.17, 279.08, 262.08, 251.08, 247.17, 223.08	306.409	koumine	indole and derivatives	MassBank PR310451
23	[M + H]+	6.38	309.20	309.17, 294.08, 291.08, 281.08, 279.08, 277.08, 265.17, 251.08	308.381	vincanidine	alkaloids	MassBank PR300706
24	[M + H]+	6.53	319.20	318.08, 290.08, 274.08, 261.08, 246, 217, 205.17	318.237	myricetin	flavonols	MassBank PR302065
25	[M + H]+	7.66	323.30	323.17, 321.08, 308.08, 305.17, 295.17, 293.17, 280.08, 267.08	322.408	gardnutine	alkaloids	MassBank PR300210
26	[M + H]+	8.48	337.20	337.08, 335.17, 309.08, 307.08, 294.17, 281.17, 279.08, 276.17	336.435	tabersonine	alkaloids	MassBank PR310588
27	[M + H]+	8.64	342.30	342.17, 311.17, 297.08, 265.08, 251.17, 192.08	341.407	isocorydine	aporphines	MassBank PR300810
28	[M + H]+	9.09	352.30	321.17, 307.08, 293.17, 277.17, 263.17	351.110673	oxoglaucine	alkaloids	MassBank BML00810
29	[M + H]+	9.20	354.30	354.17, 339.17, 336.17, 323.17, 321.17, 305.08, 293.08, 275.08, 265.17, 247.08, 235.08, 223.08, 206.08, 192.08, 188.08	353.12632	protopine	alkaloids	MassBank KO009201
30	[M + H]+	9.73	355.30	355.17, 337.17, 322.17, 276.08	354.09508	chlorogenic acid	phenylpropanoids	MassBank KO008922
31	[M + H]+	9.84	370.30	370.25, 352.08, 339.08, 291.17, 263.08, 222.17, 204.17, 165.08	369.157623	cryptopine	alkaloids	MassBank BML00793
32	[M + H]+	10.53	398.30	398.17, 380.17, 353.17, 337.17, 335.17, 322.17, 309.17, 294.17	397.427	ethylrhoeagenine	ehoeadine alkaloids	MassBank PR301718

https://doi.org/10.1021/acsomega.3c07655
ACS Omega 2024, 9, 3642−3668

Table 1. continued

sr. no.	analysis mode	rt (min)	m/z	product ions (m/z)	accurate mass	identified compound	compound class	references
33	[M + H]+	11.54	414.30	414.17, 399.17, 396.25, 382.25, 354.08, 351.08, 337.08, 321.17, 319.17	413.14745	S,R-noscapine	alkaloids	MassBank PB005907
34	[M + H]+	12.87	455.30	455.25, 356.50, 344.08, 320.17, 318.08, 303.17, 247.08	454.478	epsilon-viniferin	arylbenzofuran flavonoids	MassBank PR310521

[a]Rt: retention time; m/z: mass-to-charge ratios.

risk factors for death and morbidity; approximately nine million fatalities yearly are attributable to it.[9,10] In the United Kingdom, hypertension is defined by the NICE (National Insitute for Health and Care Excellence) as a blood pressure of 140/90 mmHg in a medical clinic or higher as assessed with follow-up ambulatory monitoring of blood pressure at home throughout the day, 135/85 mmHg or higher. It is not only elderly persons that get hypertension. In 2015, over 2.1 million persons under 45 in England had hypertension.[9]

Myocardial infarction is the leading cause of disability and mortality worldwide.[11] Myocardial infarction refers to the death of cardiac myocytes brought on by ischemia, which results from a mismatch between blood flow demand and supply.[12,13] Despite substantial advances in prognosis over the previous decade, acute MI is the most severe coronary artery disease manifestation, impacting more than seven million people worldwide and inflicting more than four million deaths annually in Northern Asia and Europe.[14,15] Oxidative stress and inflammation are the primary pathophysiological processes involved in myocardial infarction, as well-established.[16,17]

The global endeavor is to investigate treatments that prevent MI from damaging cardiac tissues. Common treatments can have unwanted consequences and require constant attention.[18] Secure, effective, and economical alternative treatments are increasingly used to alleviate various medical issues.[19] Ethnopharmacological investigations are highly relevant in manufacturing herbal remedies. Ethnopharmacology is a transdisciplinary and interdisciplinary method in drug development that comprises observing, describing, and analyzing the biological activity of traditional medicines.[20−22] Recent accomplishments in the rapidly expanding field of ethnopharmacology are numerous. Cutting-edge innovative methodologies and specialized extraction techniques have facilitated the transfer from traditional ethnopharmacology to drug discovery. The leading-edge, innovative techniques include liquid chromatography−-mass spectrometry, high-performance liquid chromatography, chemoinformatics, advancements in isolation and classification, gas chromatography−mass spectrometry, and a surge in computing capability incorporating prediction of chemical gene target and molecular docking.[23] Ethnopharmacology is a viable method for identifying bioactive compounds having a broader use beyond their original traditional usage.[24]

Medicinal herbs have been utilized to treat ischemic heart problems for centuries.[25] *Fumaria indica* (Hausskn.) Pugsley is a member of the Papaveraceae family, which is prevalent in the lower hills and plains of Pakistan, India, Turkey, Iran, Afghanistan, and Central Asia. *F. indica*, also known as Fumitory, Earth smoke, and Fumus in English, is known locally as 'Pitpapra' and 'Shahtrah'. *F. indica* has been used in alternative medicine for decades to treat cardiovascular diseases, including hypertension.[26−29] Reportedly, it possesses hepatoprotective properties,[30] spasmolytic and spasmogenic, antileishmanial, antidiabetic,[31] antianxiety, cognitive modulating activity,[32] gastroprotective,[33] anti-inflammatory,[34] chemoprotective activity,[35] antidengue,[36] and antioxidant activity.[37,38] Predominantly, isoquinoline alkaloids are responsible for these actions, with protopine being the most commonly discovered.[39] Previous research has demonstrated that protopine contains hypotensive properties, smooth muscle relaxants, and antiarrhythmic effects.[27,40] However, hydromethanolic extract of *F. indica* research on hypertension and myocardial ischemia is lacking in the scientific literature. Moreover, scientific facts supporting traditional usage and toxicity assessments of medicinal herbs persisted despite their increasing popularity and ubiquity.[41,42]

Therefore, the main aim of this study was to identify bioactive compounds via LC ESI-MS/MS analysis of *Fumaria indica* (Hausskn.) Pugsley hydromethanolic extract, hypotensive mechanism exploration based on *in vitro*, *in vivo*, and in silico studies, its cardioprotective effect investigation, and safety assessment.

2. RESULTS

2.1. Bioactive Compound Identification via LC-ESI-MS/MS Analysis. Fip.Cr LC-ESI-MS/MS analysis discovered 33 bioactive compounds, including ten alkaloids, five coumarins, four flavonoids, two phenylpropanoids, one compound of hydroxycinnamic acid, fatty acyl, gallic acid and derivative, glucosinolate, cinnamic acid and derivative, amino compound, dihydroisoquinoline, tetrahydroisoquinoline, carbazole, terpenoid, indole and derivative, and aporphine. In the negative ionization mode, Sr. No. 1−11 compounds were tentatively recognized as [M − H]− deprotonated molecules. In the positive ionization mode, Sr. No. 12−34 compounds were tentatively recognized as [M + H]+ protonated molecules (Table 1). Scopoletin was identified in both modes. Supplementary Figure S1 depicts the total ion chromatogram (TIC) containing a full scan of both positive and negative ionization modes, mass spectra (MS/MS), and chemical structures of all bioactive compounds identified.

2.2. In Vitro Experiments. *2.2.1. Effects of In Vitro Vascular Reactivity Investigations.* To evaluate the vasorelaxant effect of Fip.Cr, an intact endothelium aortic preparation, was used. In undamaged endothelium, Fip.Cr exerted a relaxing action without any constriction. Fip.Cr exhibited a minor vasoconstrictor effect on aortic-denuded preparations at lower conc. 0.01−1.0 mg/mL, followed by vasorelaxant effect at the subsequent higher conc. 3.0 mg/mL. Yohimbine (1 μM) inhibited these constrictions in aortic-denuded preparations (Figure 1).

The Fip.Cr demonstrated a complete, concentration-dependent relaxant effect on K^+ (80 mM) and phenylephrine (1 μM) evoked contractions in endothelium-intact aortic preparation at the same concentrations 1 mg/mL with the following respective EC_{50} values and 95% CI: 0.13 (0.12−0.15); and 0.24 (0.21−0.29) (Figure 2A). The Fip.Cr demonstrated a complete, concentration-dependent relaxant effect on K^+ (80 mM) and

https://doi.org/10.1021/acsomega.3c07655
ACS Omega 2024, 9, 3642−3668

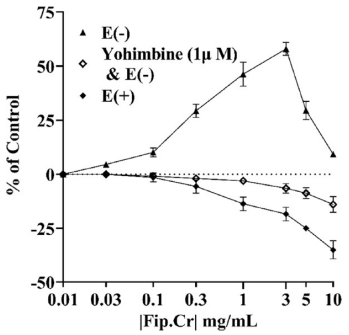

Figure 1. Effect of Fip.Cr on endothelium-intact and endothelium-denuded aortic tissue preparation.

phenylephrine (1 μM) evoked contractions in endothelium-denuded aortic preparation at the same concentrations 1 mg/mL with the following respective EC_{50} values and 95% CI: 0.15 (0.14−0.16); and 0.22 (0.20−0.25) (Figure 2B).

Endothelium-intact aortic preparation pretreatment with ten μM L-NAME exhibited a vasorelaxant effect of Fip.Cr with a corresponding EC_{50} value of 0.18 mg/mL (95% CI: 0.17−0.19) when precontracted with PE (1 μM) (Figure 2C).

These findings were validated and compared to the calcium channel blocker verapamil regarding the potential calcium antagonistic activity of Fip.Cr. Verapamil relaxed, K^+ (80 mM), and phenylephrine (1 μM) evoked contractions on endothelium-intact aortic preparation at the same concentrations 0.3 μM with respective EC_{50} values: EC_{50} 0.0398 (95% CI: 0.03503−0.04606); and EC_{50} 0.0677 (95% CI: 0.05846−0.08148) (Figure 2D).

2.2.2. Effects of In Vitro Rat Paired Atrial Study. The chronotropic and inotropic effects of Fip.Cr was studied using paired atria preparations from normal rats. The Fip.Cr has demonstrated a concentration-dependent reduction in heart rate (100%) and force of contraction (100%) at the same concentrations 0.01−0.1 mg/mL with the following respective EC_{50} values and 95% CI: 0.04 (0.03−0.06); and 0.08 (0.05−0.25) (Figure 3A). Tissues pretreated with atropine (1 μM) had a 100% reduction in heart rate and force of contraction at the same concentrations of 0.03−0.3 mg/mL with the following respective EC_{50} values and 95% CI: 0.11 (0.07−0.22); and 0.24 (0.17−0.49) (Figure 3B). Verapamil has demonstrated concentration-dependent decreases in the heart rate and force of contraction at concentrations 03 μM and 0.3 μM, respectively, with the following corresponding EC_{50} values and 95% CI: 0.3164 (0.2736−0.3770); and 0.05599 (0.04691−0.07041) (Figure 3C).

2.3. In Vivo Experiments. *2.3.1. Safety Assessment. 2.3.1.1. Observations of Clinical and Survival.* **Acute Toxicity Study**

In the acute toxicity study, neither 4 h of continuous observation nor 24 h revealed any mortalities. In addition, no lethal effects were discovered for 14 days after giving the extract during the experiment. The morphological attributes (fur, skin, eyes, and nose) were normal. There was no evidence of salivation, diarrhea, lethargy, or other abnormal behaviors. Intake of food and water, as well as respiration, were normal.

Nonetheless, modest sedation was noticed in the first 4 h following administration of the test extract, particularly at the maximum dosage of 2,000 mg/kg. The sedative effect diminished within minutes, and the rats resumed normal behavior. During the study's duration, no more harmful consequences were detected. This finding implies that Fip.Cr dosages of 1000, 1500, and 2000 mg/kg (body weight) were safe. No mortalities were documented for any dosages, so the LD_{50} value exceeded the test dose limit of 2,000 mg/kg. Therefore, oral dosages of 125, 250, and 500 mg/kg Fip.Cr were used to investigate subacute toxicity. The normal vehicle-administered control group did not experience any toxicity or fatality during the research period.

Subacute Toxicity Study

For 28 days, no mortality was observed in rats administered Fip.Cr orally at 125, 250, or 500 mg/kg bw. For the 28-day research period, none of the rats demonstrated any clinical toxicity or observable signs of morbidity, including changes in skin, eyes, hair, respiratory rate, stereotypical behaviors, and autonomic (sweating, salivation, and piloerection). The normal control group had no clinical symptoms of toxicity. Any modest changes or behaviors seen in rats throughout the research period can be categorized as typical for Sprague−Dawley rats.

2.3.1.2. Body Weight. During the experimental period of acute and subacute toxicity study, the animals treated with the extract did not exhibit significant changes in body weight and percentage of body weight gain of rats by weeks compared to the normal control (NW) group ($p > 0.05$), indicating that the extract did not affect the animals' normal growth. The findings are depicted in Table 2 and Figure S2.

2.3.1.3. Necropsy and Organ Weight. The macroscopic examinations of key organs such as the kidneys, lungs, stomach, intestines, spleen, liver, pancreas, and heart following administration of Fip.Cr at varied dosages did not reveal any notable macroscopic alterations or the development of lesions. Table 3 displays the absolute (g) and relative weight (%) of the heart, kidney, liver, spleen, and lungs. The results demonstrated that the administration of Fip.Cr at various dosages did not have a

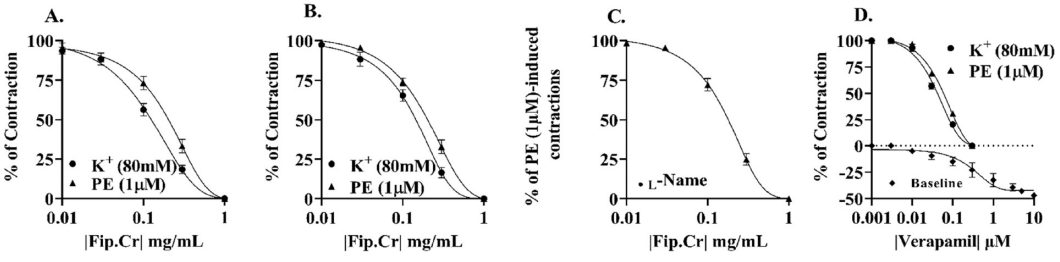

Figure 2. Effect of Fip.Cr against K^+ (80 mM) and phenylephrine (1 μM) induced contractions on (A) endothelium-intact and (B) endothelium-denuded aortic tissue preparation. (C) Vasorelaxant effect of Fip.Cr with L-NAME (10 μM) pretreatment endothelium-intact rat aorta against phenylephrine (1 μM) induced contractions. (D) Effect of verapamil against K^+ (80 mM) and phenylephrine (1 μM) induced contractions on endothelium-intact aortic tissue preparation. Values are presented as the mean ± SD (n = 5).

https://doi.org/10.1021/acsomega.3c07655
ACS Omega 2024, 9, 3642−3668

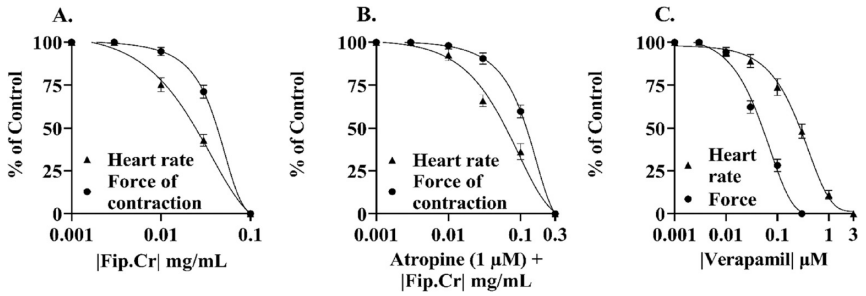

Figure 3. Concentration−response curves illustrate the effect of Fip.Cr on heart rate and force of contraction in rat atrial preparation (A) in the absence and (B) in the presence of atropine (1 μM). (C) Effect of verapamil on heart rate and force of contraction in rat atrial preparation. Values are presented as the mean ± SD (n = 5).

Table 2. Evaluating Body Weight and Weight Gain Percentage in Acute and Subacute Toxicity Studies of Rats with Fip.Cr Treatment[a]

	acute toxicity				subacute toxicity			
parameters	normal control group	1000 mg/kg	1500 mg/kg	2000 mg/kg	normal control group	125 mg/kg	250 mg/kg	500 mg/kg
				Body Weight				
initial weight (g)	191 ± 18.40	187 ± 12.83	193.2 ± 14.92	188 ± 10.54	194.2 ± 14.72	185.4 ± 11.28	183.8 ± 7.29	185.8 ± 6.72
7th day (g)	202 ± 21.45	196.6 ± 12.01	197.8 ± 17.88	193.4 ± 11.63	201.4 ± 16.99	195 ± 10.49	191 ± 10.98	192 ± 7.62
14th day (g)	210.8 ± 23.48	205.4 ± 13.35	204.6 ± 17.56	200.6 ± 12.42	210 ± 18.43	200 ± 12.69	202.2 ± 11.34	203.4 ± 6.19
21st day (g)					222.8 ± 16.86	210.2 ± 12.87	210.8 ± 9.731	213.4 ± 10.24
28th day (g)					236.8 ± 16.90	219.6 ± 13.26	222.4 ± 11.48	226 ± 9.43
				Body Weight Gain				
7th day (%)	5.69 ± 2.15	5.19 ± 2.20	2.30 ± 1.8	2.87 ± 2.19	3.66 ± 1.48	5.23 ± 2.57	3.88 ± 2.75	3.34 ± 1.89
14th day (%)	10.27 ± 3.13	9.91 ± 3.28	5.88 ± 2.95	6.73 ± 3.96	8.06 ± 2.25	7.89 ± 2.99	9.99 ± 4.10	9.53 ± 2.62
21st day (%)					14.73 ± 1.49	13.41 ± 3.59	14.74 ± 4.61	14.98 ± 7.12
28th day (%)					21.98 ± 2.47	18.51 ± 4.58	21.01 ± 4.4	21.75 ± 6.53

[a](n = 5) Values are reported as mean ± standard deviation. One-way ANOVA followed by Dunnett's t test for statistical analysis. *p < 0.05 compared to the control group.

Table 3. Evaluation of Absolute Organ Weight (g) and Relative Organ Weight Percentage in Acute and Subacute Toxicity Studies Treatment of Rats with Fip.Cr[a]

		acute toxicity				subacute toxicity			
organ		normal control group	1000 mg/kg	1500 mg/kg	2000 mg/kg	normal control group	125 mg/kg	250 mg/kg	500 mg/kg
heart	absolute	0.76 ± 0.12	0.76 ± 0.04	0.71 ± 0.09	0.70 ± 0.13	0.80 ± 0.15	0.76 ± 0.15	0.71 ± 0.11	0.80 ± 0.10
	relative	0.36 ± 0.02	0.37 ± 0.01	0.35 ± 0.02	0.35 ± 0.05	0.34 ± 0.05	0.35 ± 0.05	0.32 ± 0.04	0.35 ± 0.03
kidney	absolute	0.84 ± 0.19	0.82 ± 0.07	0.80 ± 0.13	0.76 ± 0.10	0.90 ± 0.26	0.78 ± 0.12	0.86 ± 0.19	0.97 ± 0.20
	relative	0.39 ± 0.04	0.40 ± 0.01	0.39 ± 0.04	0.38 ± 0.03	0.38 ± 0.09	0.36 ± 0.05	0.39 ± 0.07	0.43 ± 0.07
liver	absolute	6.20 ± 1.3	6.28 ± 1.3	6.10 ± 1.2	5.42 ± 0.84	6.82 ± 1.43	6.25 ± 1.14	7.19 ± 0.56	7.02 ± 0.87
	relative	2.93 ± 0.45	3.04 ± 0.49	2.97 ± 0.36	2.70 ± 0.36	2.86 ± 0.42	2.85 ± 0.48	3.24 ± 0.29	3.11 ± 0.35
spleen	absolute	0.58 ± 0.20	0.54 ± 0.11	0.49 ± 0.11	0.50 ± 0.12	0.50 ± 0.13	0.44 ± 0.13	0.48 ± 0.09	0.53 ± 0.17
	relative	0.27 ± 0.07	0.26 ± 0.03	0.24 ± 0.04	0.25 ± 0.05	0.21 ± 0.04	0.20 ± 0.05	0.22 ± 0.04	0.23 ± 0.07
lungs	absolute	1.54 ± 0.45	1.71 ± 0.39	1.65 ± 0.32	1.31 ± 0.37	1.92 ± 0.28	1.49 ± 0.20	1.56 ± 0.35	1.73 ± 0.22
	relative	0.72 ± 0.14	0.83 ± 0.13	0.80 ± 0.10	0.65 ± 0.15	0.81 ± 0.06	0.68 ± 0.05	0.70 ± 0.14	0.76 ± 0.07

[a]The presented values (n = 5) are the mean ± standard deviation. For statistical analysis, one-way ANOVA was followed by Dunnett's t test. *p < 0.05 concerning the control group.

notable harmful effect on the macroscopic examination of vital organs and the absolute and relative organ weights of selected organs compared to the normal control (NW) group (p > 0.05). This finding might corroborate the safety of Fip.Cr extract administered in doses up to 2,000 mg/kg orally, as the relative weight of organs can be altered by hazardous chemicals.[43]

2.3.1.4. Hematological Analysis. Compared to the normal control group, all parameters exhibited statistically insignificant and dose-independent alterations (p > 0.05) (Table 4).

2.3.1.5. Biochemical Analysis. Compared to the normal control group, all parameters exhibited statistically insignificant and dose-independent alterations (p > 0.05) (Table 4).

2.3.1.6. Histopathological Studies. Comparative histopathological analysis of rats' hearts, livers, kidneys, and lungs revealed no major and significant alterations from the normal control group (Figure 4).

2.3.2. Effect on Blood Pressure and Hemodynamic Parameters. At dosages of 10, 20, and 30 mg/kg, Fip.Cr

https://doi.org/10.1021/acsomega.3c07655
ACS Omega 2024, 9, 3642−3668

Table 4. Effects on Hematological and Biochemical Parameters of Fip.Cr's Acute and Subacute Toxicities Assessments in Rats[a]

parameters	normal control group	acute toxicity			subacute toxicity		
		1000 mg/kg	1500 mg/kg	2000 mg/kg	125 mg/kg	250 mg/kg	500 mg/kg
TLC/WBC count × $10^3/\mu L$	6.29 ± 1.32	5.90 ± 1.32	6.78 ± 1.79	6.29 ± 1.19	5.98 ± 1.48	6.88 ± 2.19	6.72 ± 1.63
RBC count × $10^6/\mu L$	7.52 ± 0.59	7.82 ± 1.10	8.05 ± 0.38	8.15 ± 0.93	7.77 ± 0.92	7.83 ± 0.99	8.16 ± 1.22
hemoglobin (Hb%) g/dL	13.7 ± 1.00	14.4 ± 0.96	13.1 ± 1.09	12.5 ± 1.45	14.2 ± 2.10	12.8 ± 1.97	13.3 ± 1.29
HCT (PCV) %	41.5 ± 3.53	41.7 ± 1.67	42.0 ± 3.04	44.9 ± 2.93	42.2 ± 2.61	40.7 ± 2.54	43.2 ± 4.32
MCV fL	53.4 ± 1.26	54.9 ± 2.15	55.4 ± 1.93	54.6 ± 1.42	54.1 ± 1.61	54.7 ± 2.21	56.3 ± 3.00
MCH Pg	18.0 ± 1.21	18.8 ± 1.86	19.3 ± 1.44	18.5 ± 1.43	18.6 ± 1.41	18.9 ± 1.64	17.5 ± 1.93
MCHC g/dL	33.1 ± 2.35	33.6 ± 1.59	33.3 ± 2.27	33.3 ± 1.19	32.7 ± 1.76	32.2 ± 3.33	31.8 ± 1.69
platelets × $10^3/\mu L$	729 ± 90.5	718 ± 76.4	859 ± 96.3	874 ± 108	709 ± 66.8	865 ± 112	878 ± 103
neutrophils %	26.71 ± 2.54	28.65 ± 3.77	27.71 ± 4.11	25.36 ± 5.6	26.09 ± 4.70	25.65 ± 2.72	23.48 ± 3.46
lymphocytes %	74.48 ± 3.47	72.68 ± 5.013	73.81 ± 2.974	76.68 ± 2.66	72.67 ± 4.05	75.11 ± 3.6	77.54 ± 2.113
monocytes %	0.75 ± 0.11	0.78 ± 0.21	0.83 ± 0.13	0.86 ± 0.14	0.88 ± 0.29	0.90 ± 0.25	0.92 ± 0.14
eosinophils %	1.14 ± 0.29	1.02 ± 0.22	1.05 ± 0.21	1.13 ± 0.14	1.03 ± 0.34	1.07 ± 0.24	1.10 ± 0.20
glucose random mg/dL	83.40 ± 5.77	82.40 ± 2.79	79.20 ± 4.03	77.00 ± 2.92	81.40 ± 4.67	80.00 ± 7.65	78.60 ± 3.91
bilirubin total mg/dL	0.75 ± 0.21	0.76 ± 0.15	0.73 ± 0.11	0.69 ± 0.13	0.78 ± 0.16	0.77 ± 0.13	0.74 ± 0.17
SGPT (ALT) U/L	53.20 ± 7.86	56.20 ± 6.26	58.80 ± 7.63	63.00 ± 4.85	54.40 ± 6.88	57.20 ± 4.60	61.20 ± 5.72
SGOT (AST) U/L	150.8 ± 11.08	147.6 ± 8.99	142.8 ± 11.43	140.2 ± 15.16	148.2 ± 13.39	144.4 ± 14.21	143.6 ± 16.86
alkaline phosphatase U/L	250.6 ± 4.62	254.8 ± 7.09	252.6 ± 4.83	244.2 ± 6.98	253.4 ± 6.39	251.8 ± 5.63	247.4 ± 8.62
blood urea mg/dL	20.60 ± 3.85	17.80 ± 4.09	14.20 ± 3.83	18.20 ± 5.54	19.40 ± 5.86	15.20 ± 2.59	19.20 ± 2.78
serum creatinine mg/dL	0.90 ± 0.09	0.88 ± 0.03	0.84 ± 0.04	0.79 ± 0.10	0.89 ± 0.06	0.86 ± 0.05	0.82 ± 0.07
sodium mmol/L	145.4 ± 4.88	149.4 ± 5.13	144.8 ± 5.45	146.8 ± 4.49	150.6 ± 6.88	147.2 ± 7.36	152.4 ± 5.77
potassium mmol/L	5.51 ± 0.88	4.47 ± 0.85	5.33 ± 0.54	5.49 ± 0.41	4.65 ± 0.46	5.74 ± 0.59	5.62 ± 0.76
chloride mmol/L	104.2 ± 5.45	110.4 ± 9.15	105.2 ± 6.02	99.20 ± 5.02	108.4 ± 8.65	107.2 ± 7.05	102.6 ± 6.43
total cholesterol mg/dL	87.80 ± 5.59	80.60 ± 3.78	83.80 ± 5.36	88.80 ± 4.15	79.60 ± 4.62	86.40 ± 7.34	91.40 ± 4.72
triglycerides mg/dL	120.4 ± 4.34	116.4 ± 5.27	112.0 ± 6.042	119.6 ± 4.88	118.2 ± 3.83	109.0 ± 9.35	115.2 ± 8.70
LDL cholesterol mg/dL	22.40 ± 3.44	20.80 ± 2.28	22.20 ± 3.11	26.60 ± 3.36	21.60 ± 2.7	23.40 ± 2.51	24.20 ± 4.21
HDL cholesterol mg/dL	49.40 ± 4.34	48.60 ± 3.85	51.20 ± 4.82	52.20 ± 4.49	50.00 ± 6.6	50.40 ± 5.94	53.80 ± 5.02
total protein g/dL	6.62 ± 0.51	5.9 ± 0.47	6.32 ± 0.64	7.14 ± 0.47	6.22 ± 0.29	6.92 ± 0.79	6.50 ± 0.66
albumin g/dL	3.22 ± 0.26	2.98 ± 0.28	3.32 ± 0.42	3.74 ± 0.54	3.54 ± 0.32	3.48 ± 0.46	3.70 ± 0.33

[a]All data are means ± standard deviation ($n = 5$) and analyzed through one-way ANOVA followed by Dunnett's t test compared with the normal control group. Values of $^*p < 0.05$ were considered significant.

lowered MABP by 101.3 ± 3.8, 99.21 ± 1.2, and 94.31 ± 2.6, respectively. The hypotensive response to 10, 20, and 30 mg/kg Fip.Cr was dose-dependent. In normotensive anesthetized rats, Fip.Cr intravenous administration decreased dose-dependent systolic (SBP) and diastolic blood pressure (DBP), along with a reduction in pulse pressure and heart rate (BPM) (Figure 5A). At dosages of 1, 3, and 10 μg/kg, verapamil lowered MABP in normotensive anesthetized rats by 95 ± 5.1, 82.90 ± 3.9, and 62.23 ± 2.0, respectively (Figure 5B).

2.3.3. Effect of Fip.Cr on Isoproterenol-Induced Chronic Myocardial Infarction. Fip. Cr's effect on isoproterenol-induced chronic myocardial infarction was investigated using several preclinical cardiac hypertrophy measures, such as biometrical indices, cardiac biochemical markers, and histological parameters. It was discovered that Fip.Cr protected the rats from chronic myocardial damage generated by ISO.

2.3.3.1. Physical Activity and Life Expectancy. During the research, significant heart failure or myocardial infarction indicators include survival rate and physical activity. Myocardial ischemia is anticipated to cause death throughout this research. Rats administered verapamil, carvedilol, and Fip.Cr (100 and 200 mg/kg) did not perish. Myocardial infarction caused the death of one out of five rats in the IC (ISO) group.

The physical activity of rats decreased in this investigation after the fourth dose of subcutaneous isoproterenol in the intoxicated (ISO) group, and the decline was complete by the tenth treatment, which was accompanied by a decrease in respiration, while the verapamil, carvedilol, and Fip.Cr (100 and 200 mg/kg)-treated rats had mild breathlessness and were active. During the investigation, observations revealed that rats in the IC group lost weight, and their weariness and shortness of breath worsened. Rats treated with verapamil, carvedilol, and Fip.Cr (100 and 200 mg/kg) did not experience weight loss, worsening weariness, or shortness of breath.

2.3.3.2. Effect on Biometrical Indicators. The effect of Fip.Cr on the biometric indicators of ISO-induced heart hypertrophy is depicted in Figure 6A. The IC group had significantly increased ($p < 0.05$ vs NC group) heart and left ventricular heart (LVH) weight, heart diameter, tail and tibia length index, and heart and LVH weight index. The biometrical indicators were lowered by verapamil, carvedilol, and Fip.Cr (100 and 200 mg/kg). These treated groups demonstrated significant protection ($p < 0.05$ vs IC group) against heart hypertrophy. The treatment groups did not differ statistically significantly from the normal control group ($p > 0.05$ vs NC group). Fip.Cr low dosage (100 mg/kg) was observed to provide marginal protection ($p < 0.05$ vs IC group) in rats with modest statistical significance.

2.3.3.3. Effect on Cardiac Serum Biochemical Indicators. CPK, CK-MB, lipid profile, LDH, cTnT, and ANP are biochemical serum markers of diagnostic significance for myocardial infarction. In addition, various blood indicators, such as AST, ALT, and serum IL-6 aid in research on heart damage. Figure 6B demonstrates a statistically significant

https://doi.org/10.1021/acsomega.3c07655
ACS Omega 2024, 9, 3642−3668

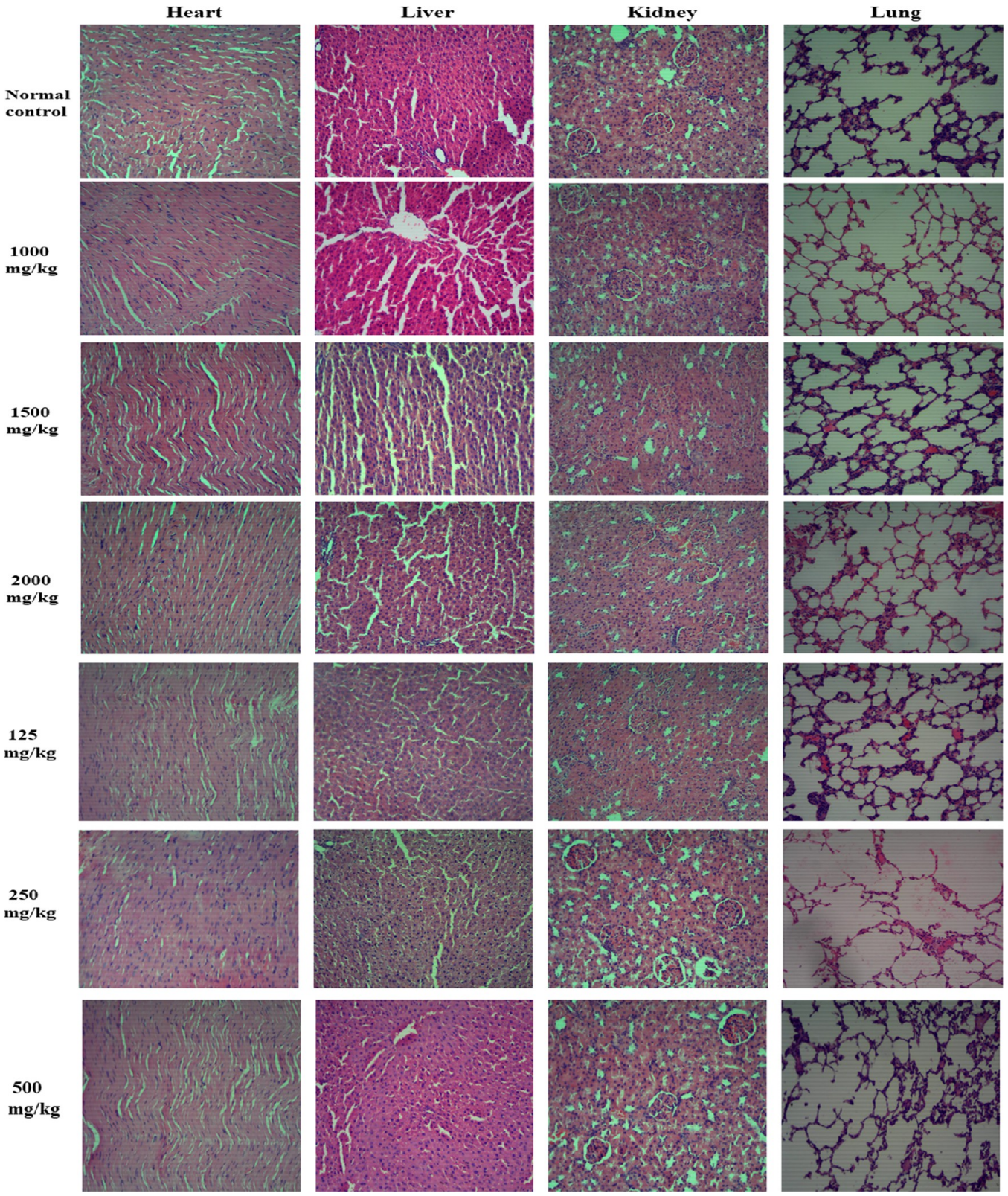

Figure 4. Photomicrographs of histopathological findings of hearts, liver, kidneys, and lungs from rats treated with normal control vehicle and Fip.Cr at acute and subacute doses (1000, 1500, 2000, 125, 250, and 500 mg/kg, b.wt.) for 14 and 28 days, respectively (H&E staining, 10× magnification).

distinction between control and IC (ISO) biomarkers ($p < 0.05$ vs NC group); increasing these biomarkers in the ISO-administered group implies persistent MI. Although carvedilol, verapamil, and Fip.Cr (100 and 200 mg/kg) groups exhibited blood biomarkers within the permissible range. These treated groups demonstrated significant protection ($p < 0.05$ vs IC group) against MI. The treatment groups did not differ statistically significantly from the normal control group ($p > 0.05$ vs NC group). These findings demonstrated that Fip.Cr protects rats against the cardiotoxicity generated by ISO.

https://doi.org/10.1021/acsomega.3c07655
ACS Omega 2024, 9, 3642−3668

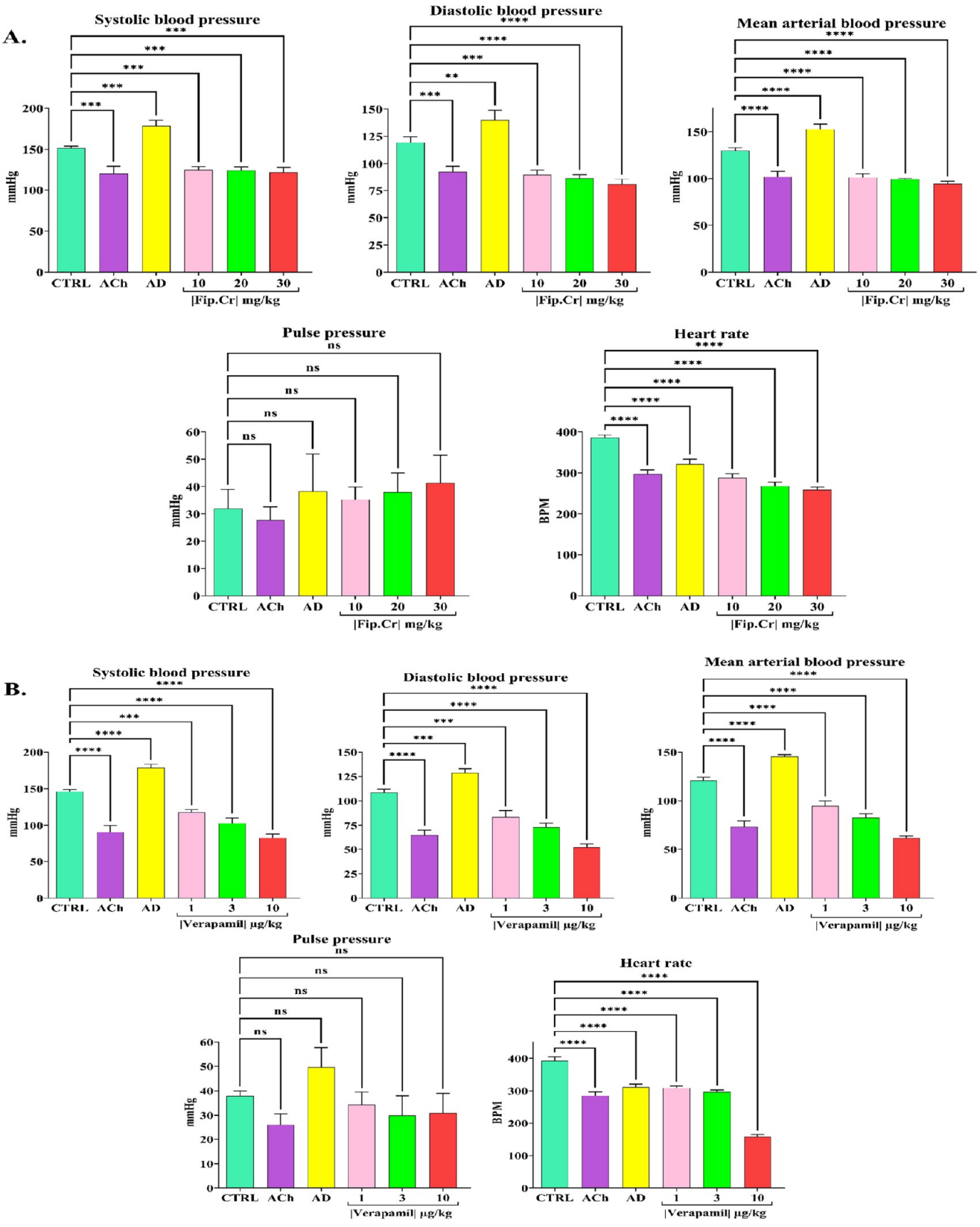

Figure 5. Effect of (A) Fip.Cr 10, 20, and 30 mg/kg and (B) verapamil 1, 3, and 10 μg/kg on normotensive blood pressure. Values are presented as the mean ± SD (n = 3−4) and analyzed through one-way ANOVA followed by the Dunnett test compared with the control group. Values of $^{**}p < 0.01$, $^{***}p < 0.001$, $^{****}p < 0.0001$ were considered significant. ns = nonsignificant. CTRL: control; Ach: acetylcholine; AD: adrenaline.

Values are presented as the mean ± SD (n = 5) and analyzed through one-way ANOVA followed by the Dunnett test. Significant difference: #$p < 0.05$, ##$p < 0.01$, ###$p < 0.001$, ####$p < 0.0001$ compared with the control group; and *$p <$

https://doi.org/10.1021/acsomega.3c07655
ACS Omega 2024, 9, 3642−3668

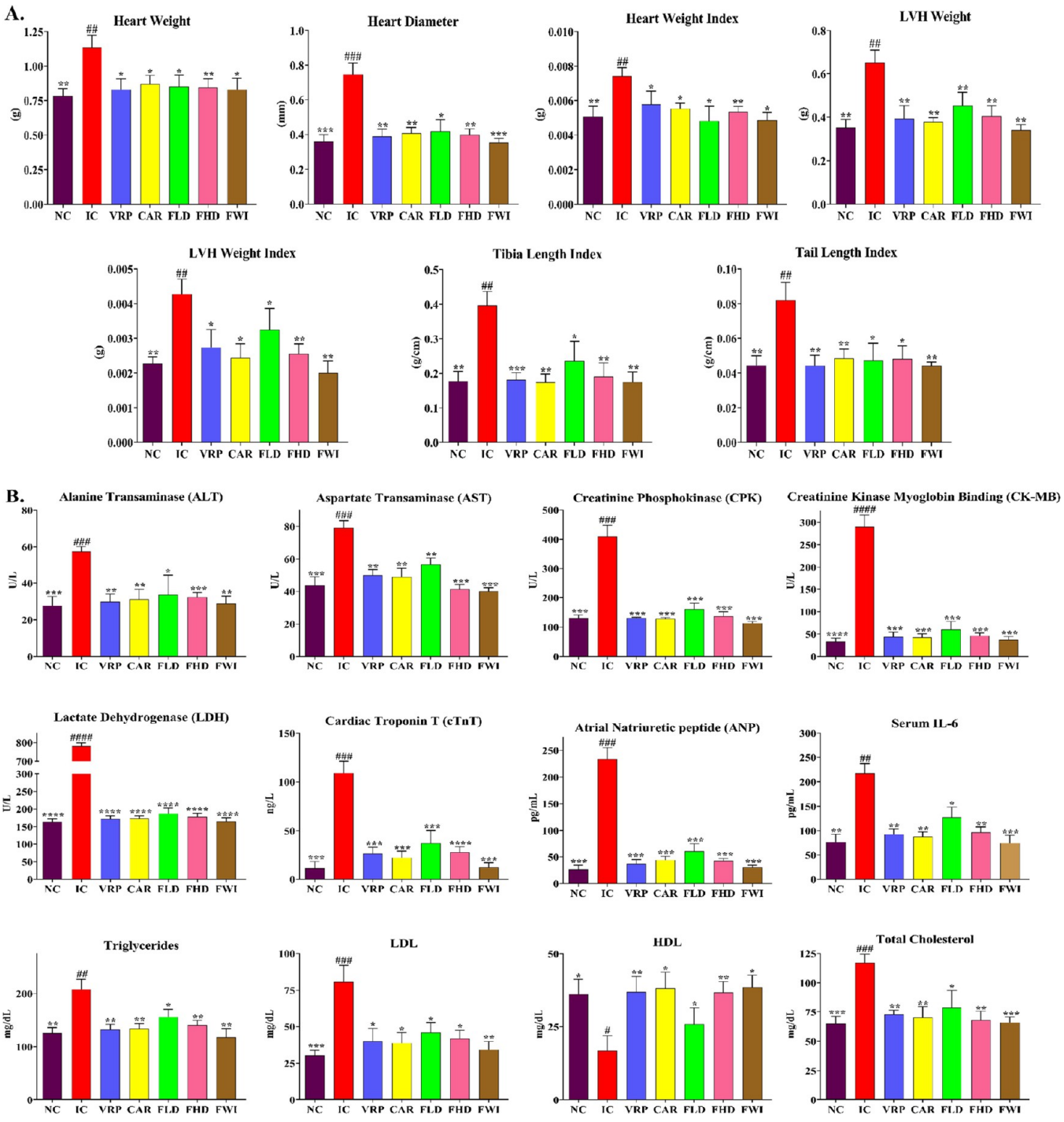

Figure 6. Effects of Fip.Cr on cardiac (A) hypertrophy biometric and (B) serum biochemical indicators in myocardial infarction.

0.05, **$p < 0.01$, ***$p < 0.001$, **** $p < 0.0001$ compared with the ISO group. NC: negative control; IC: intoxicated control (ISO: isoprenaline); VRP: verapamil; CAR: carvedilol; FLD: Fip.Cr 100 mg/kg; FHD: Fip.Cr 200 mg/kg; FWI: Fip.Cr 200 mg/kg without isoprenaline-induced MI.

2.3.3.4. Effect of Fip.Cr on the NLRP3 Inflammasome Activation, TNF-α, IL-1β, and IL-6 in Rats Induced by ISO. To determine if Fip.Cr ameliorated ISO-induced myocardial injury mediated by the NLRP3 inflammasome, the ASC, NLRP3, and caspase-1, as well as TNF-α, IL-1β, and IL-6; mRNA expression levels were measured in the hearts of all experimental groups. ISO injection manifestly activated NLRP3 inflammasome, as seen by significantly elevated mRNA expression levels of ASC, NLRP3, caspase-1, TNF-α, IL-1β, and IL-6 in cardiac tissue ($p < 0.05$ vs NC group). The treatment groups did not differ statistically significantly from the normal control group ($p > 0.05$ vs NC group). Fip.Cr significantly lowered mRNA levels of ASC, NLRP3, caspase-1, TNF-α, IL-1β, and IL-6 compared to the ISO group ($p < 0.05$ vs IC group) (Figure 7A).

2.3.3.5. Effect of Fip.Cr on Microbiota Analysis of Firmicutes and Lactobacillus. Firmicutes and Lactobacillus levels in stool samples were considerably lower in the ISO-treated group, but V2 levels were significantly elevated ($p < 0.05$ vs NC group). The treatment groups did not differ statistically

https://doi.org/10.1021/acsomega.3c07655
ACS Omega 2024, 9, 3642−3668

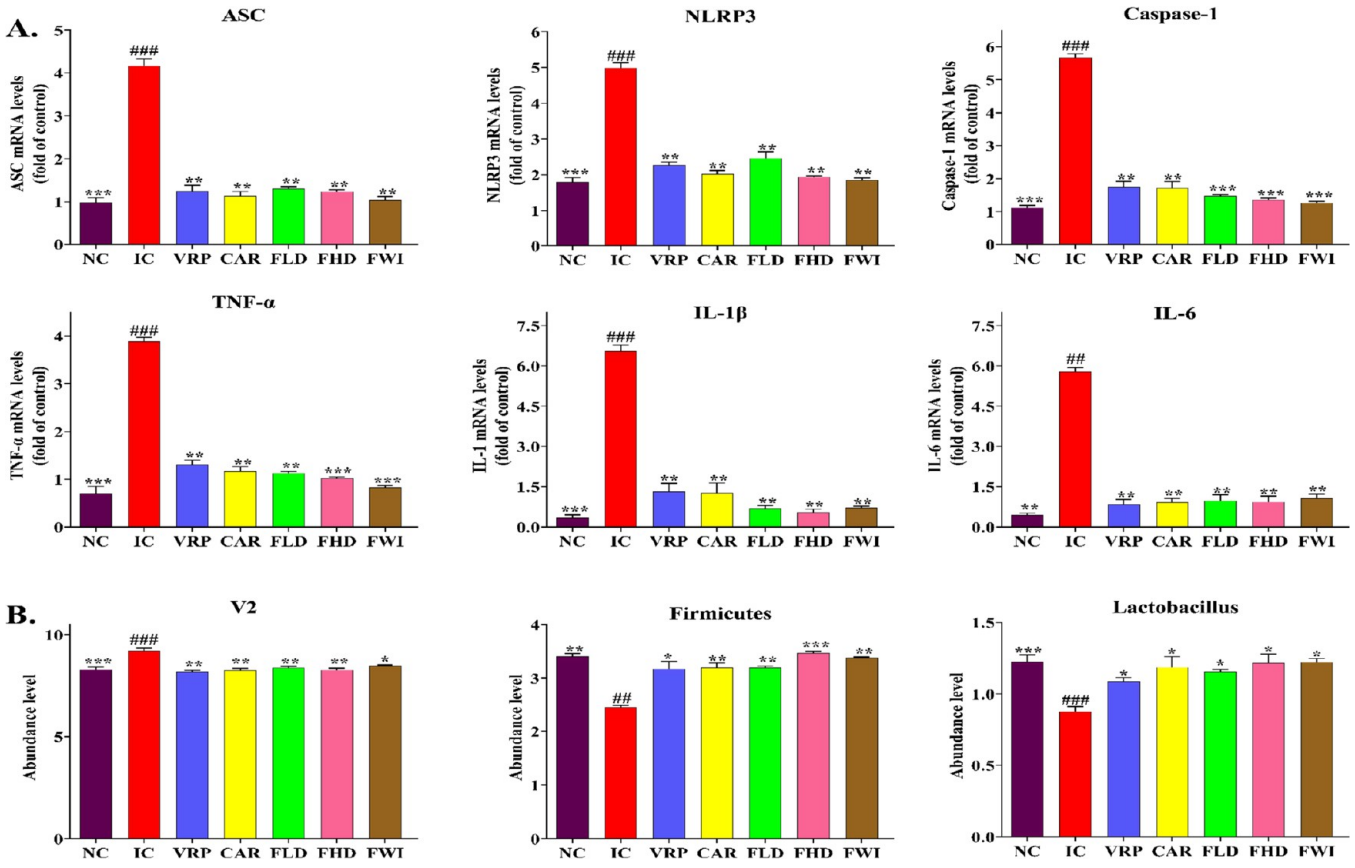

Figure 7. (A) mRNA levels of cardiac NOD-like receptor superfamily: ASC, NLRP3 (pyrin domain containing 3), and caspase-1; and TNF-α, IL-1β, and IL-6 mRNA levels; (B) abundance level of V2, Firmicutes and Lactobacillus. Values are presented as the mean ± SD (n = 3−4) and analyzed through one-way ANOVA followed by the Dunnett test. Significant difference: #p < 0.05, ##p < 0.01 compared with the control group; and *p < 0.05, **p < 0.01, ***p < 0.001 compared with the ISO group. NC: negative control; IC: intoxicated control (ISO: isoprenaline); VRP: verapamil; CAR: carvedilol; FLD: Fip.Cr 100 mg/kg; FHD: Fip.Cr 200 mg/kg; FWI: Fip.Cr 200 mg/kg without isoprenaline-induced MI.

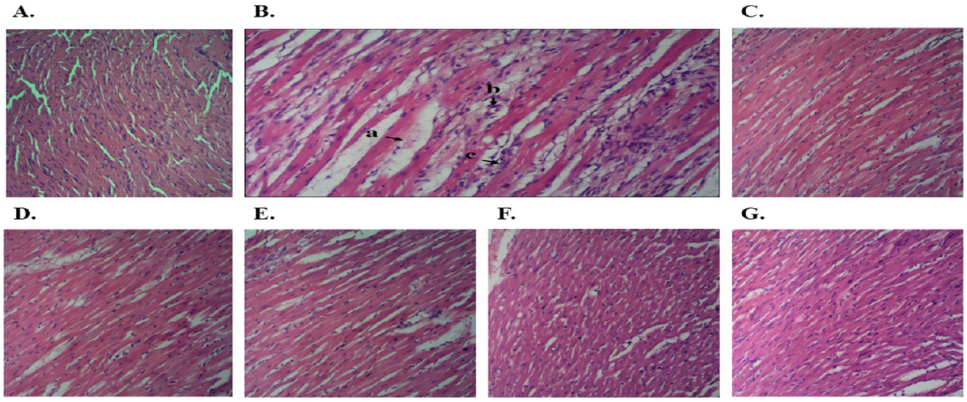

Figure 8. Photomicrographs of myocardial tissues from all experimentally treated groups (H&E staining, 10× magnification). (A) Negative control group showed normal cardiac architecture. (B) ISO-administered group exhibited (a) necrosis accompanied by (b) inflammatory cell infiltration and (c) local tissue interstitial edema (black arrows). The groups (C) Verapamil, (D) Carvedilol, (E) Fip.Cr 100 mg/kg, and (F) Fip.Cr 200 mg/kg ameliorated ISO-induced myocardial infarction damage, as shown by a substantial decrease in histological abnormalities. (G) Fip.Cr 200 mg/kg without isoprenaline-induced MI group exhibited no major histopathological alterations compared to the control group.

significantly from the normal control group (p > 0.05 vs NC group). Fip.Cr considerably boosted the levels of Firmicutes and Lactobacillus while dramatically decreasing the amounts of V2 compared to the ISO group (p < 0.05 vs IC group) (Figure 7B).

2.3.3.6. Effect of Fip.Cr on Histopathology. Histopathological analysis of the negative control group indicated normal architecture, but rats treated with ISO exhibited substantial necrosis, inflammatory cell infiltration, and local tissue interstitial edema. Rats treated with verapamil, carvedilol, and Fip.Cr at 100 and 200 mg/kg doses had a marked and maximum reduction in histological abnormalities. The Fip.Cr 200 mg/kg group without isoprenaline-induced MI had no significant histological abnormalities compared to the control group (Figure 8).

2.4. In Silico Investigations. *2.4.1. Drug-Likeness and ADMET.* The drug-likeness and ADMET analysis findings are

https://doi.org/10.1021/acsomega.3c07655
ACS Omega 2024, 9, 3642−3668

Table 5. Physiochemical Characteristics, ADME, and Drug-Likeness Parameters Generated by SWISS ADME and ADMETlab 2.0[a]

	physiochemical characteristics				ADME								drug-likeness					
molecule	nRB	nHB A	nHB D	TPSA (A^2)	GI ABS	P-gp SUB	VD L/kg	CYP2C9 INH	CYP2D6 INH	CYP3A4 INH	CL mL/min/kg	$T_{1/2}$ (h)	LIPVIO	GHO VIO	VEB VIO	EGA VIO	MUE VIO	F (%)
umbelliferone	0	3	1	50.44	high	no	0.603	no	no	no	13.575	0.834	yes	1	yes	yes	1	0.55
2-coumaric acid	2	3	2	57.53	high	no	0.276	no	no	no	4.228	0.909	yes	yes	yes	yes	1	0.85
daphnetin	0	4	2	70.67	high	no	0.551	no	no	no	16.080	0.890	yes	1	yes	yes	1	0.55
scopoletin	1	4	1	59.67	high	no	0.689	no	no	no	13.312	0.850	yes	yes	yes	yes	1	0.55
sinapic acid	4	5	2	75.99	high	no	0.450	no	no	no	7.776	0.933	yes	yes	yes	yes	yes	0.56
koumidine	1	2	2	39.26	high	yes	2.698	no	yes	no	11.457	0.228	yes	yes	yes	yes	yes	0.55
3,7-dihydroxy-3′,4′-dimethoxyflavone	3	6	2	89.13	high	no	0.712	yes	yes	yes	6.184	0.885	yes	yes	yes	yes	yes	0.55
bergenin	2	9	5	145.91	low	no	0.684	no	no	no	4.946	0.761	yes	1	1	1	yes	0.55
(methylsulfanyl)butyl glucosinolate	10	10	5	225.09	low	yes	0.895	no	no	no	1.030	0.443	yes	yes	1	1	1	0.11
isomajdine	4	8	1	89.82	high	no	1.333	no	yes	no	8.770	0.344	yes	yes	yes	yes	yes	0.55
p-coumaraldehyde	2	2	1	37.30	high	no	1.048	no	no	no	10.138	0.897	yes	2	yes	yes	1	0.55
eugenol	3	2	1	29.46	high	no	0.833	no	no	no	14.042	0.887	yes	yes	yes	yes	1	0.55
dehydrosalsolidine	2	3	0	30.82	high	no	1.421	no	no	no	9.037	0.740	yes	yes	yes	yes	yes	0.55
scoparone	2	4	0	48.67	high	no	0.882	no	no	no	11.015	0.814	yes	yes	yes	yes	yes	0.55
hydrocotarnine	1	4	0	30.93	high	yes	2.468	no	yes	no	13.790	0.586	yes	yes	yes	yes	yes	0.55
ellipticine	0	1	1	28.68	high	yes	1.235	no	yes	yes	7.423	0.275	yes	yes	yes	yes	yes	0.55
hulupinic acid	4	4	2	74.60	high	no	1.186	no	no	no	6.840	0.177	yes	yes	yes	yes	yes	0.85
2′,5-dimethoxyflavone	0	1	1	20.23	high	no	0.935	no	no	no	11.898	0.398	yes	yes	yes	yes	2	0.55
koumine	1	3	0	24.83	high	no	2.871	no	yes	yo	4.046	0.052	yes	yes	yes	yes	yes	0.55
vincanidine	1	3	2	52.57	high	yes	2.051	no	yes	yo	11.548	0.360	yes	yes	yes	yes	yes	0.55
myricetin	1	8	6	151.59	low	no	0.633	no	no	yes	7.716	0.945	1	yes	1	1	2	0.55
gardnutine	1	3	1	37.49	high	yes	3.279	no	yes	no	5.545	0.111	yes	yes	yes	yes	yes	0.55
tabersonine	3	3	1	41.57	high	yes	1.560	yes	yes	yes	7.066	0.144	yes	yes	yes	yes	yes	0.55
isocorydine	3	5	1	51.16	high	yes	1.489	no	yes	yes	7.697	0.404	yes	yes	yes	yes	yes	0.55
oxoglaucine	4	6	0	66.88	high	no	0.879	yes	yes	yes	6.990	0.418	yes	yes	yes	yes	yes	0.55
protopine	0	6	0	57.23	high	yes	2.131	yes	yes	yes	16.684	0.229	yes	yes	yes	yes	yes	0.55
chlorogenic acid	5	9	6	164.75	low	no	0.351	no	no	no	3.251	0.928	1	1	1	1	2	0.11
cryptopine	2	6	0	57.23	high	yes	2.005	yes	yes	yes	14.039	0.446	yes	yes	yes	yes	yes	0.55
ethylrhoeagenine	2	7	0	58.62	high	no	1.557	no	yes	yes	11.629	0.072	yes	yes	yes	yes	yes	0.55
S,R-noscapine	4	8	0	75.69	high	no	1.543	yes	yes	yes	5.492	0.127	yes	yes	yes	yes	yes	0.55
epsilon-viniferin	4	6	5	110.38	high	no	0.816	yes	no	no	11.765	0.681	yes	1	yes	yes	1	0.55

[a]nRB: num. rotatable bonds; nHB A: num. H-bond acceptors; nHB D: num. H-bond donors; TPSA: topological polar surface area; GI ABS: gastrointestinal absorption; P-gp SUB: P-glycoprotein substrate; VD: volume distribution, optimal 0.04-20L/kg; CYP INH: cytochrome P450 inhibitor; CL: clearance, high >15 mL/min/kg; LIP VIO: lipinski, YES is 0 violation; GHO VIO Ghose; VEB VIO: Veber; EGA VIO: Egan; MUE VIO: Muegge; F: bioavailability score.

https://doi.org/10.1021/acsomega.3c07655
ACS Omega 2024, 9, 3642−3668

Table 6. ADMET Analysis Based on QikProp and AdmetSAR[a]

molecule	CNS PERM	QPlog P o/w	QPlog HERG	QPlog Khsa	QPlog Kp	QPP Caco	QPP MDCK	QPlog S	QPlog BB	% human oral absorption	rule of five	HIA	AMES mutagenesis	acute oral toxicity rat LD50 log (1/(mol/kg))	SS
umbelliferone	−1	0.709	−3.749	−0.512	−2.991	623.262	296.765	−1.42	−0.479	81.115	0	+	-	1.52	-
2-coumaric acid	−1	1.474	−2.241	−0.674	−3.406	75.593	38.597	−1.629	−0.992	69.196	0	+	-	1.333	+
daphnetin	−1	0.139	−3.685	−0.589	−3.85	230.462	101.25	−1.347	−0.909	70.043	0	+	-	1.53	-
scopoletin	0	0.854	−3.781	−0.481	−3.065	632.798	301.676	−1.742	−0.571	82.085	0	+	-	1.036	-
sinapic acid	−2	1.534	−2.239	−0.565	−3.754	64.024	32.254	−2.215	−1.283	68.255	0	+	-	1.505	-
koumidine	1	2.844	−5.286	0.408	−4.071	511.682	265.273	−3.254	0.202	92.081	0	+	+	1.847	-
3,7-dihydroxy-3′,4′-dimethoxyflavone	−2	2.131	−5.275	−0.009	−3.056	392.776	180.164	−3.927	−1.088	85.856	0	+	-	1.611	-
bergenin	−2	−1.567	−3.698	−0.924	−5.392	36.307	13.736	−1.723	−2.06	45.691	0	-	+	1.911	-
(methylsulfanyl) butyl glucosinolate	−2	−0.614	−2.55	−1.483	−5.044	6.249	5.817	−1.56	−2.931	37.593	0	-	-	1.662	-
isomajdine	1	2.201	−5.721	0.066	−4.849	260.011	127.616	−3.763	−0.254	83.059	0	+	-	2.947	-
p-coumaraldehyde	−1	1.676	−3.995	−0.493	−3.053	473.789	220.646	−1.636	−0.818	84.644	0	+	-	2.262	+
eugenol	0	2.662	−3.958	−0.107	−1.616	3043.597	1647.534	−2.389	−0.129	100	0	+	-	2.02	+
dehydrosalsolidine	1	2.752	−3.688	0.001	−1.288	6380.057	3666.655	−2.901	0.214	100	0	+	-	1.949	-
scoparone	0	1.395	−3.786	−0.592	−2.125	2055.611	1077.959	−1.549	−0.143	94.409	0	+	-	1.464	-
hydrocotarnine	2	1.363	−3.738	−0.498	−3.389	2126.531	1237.098	−0.481	0.848	94.485	0	+	+	2.082	-
ellipticine	1	3.79	−4.813	0.544	−1.273	3817.719	2104.802	−4.402	0.192	100	0	+	+	1.751	-
hulupinic acid	−2	0.943	−3.759	−0.502	−3.782	357.816	162.896	−2.504	−1.085	78.17	0	+	-	2.104	+
2′,5-dimethoxyflavone	1	3.227	−4.906	0.231	−0.994	3557.947	1950.435	−3.288	0.117	100	0	+	+	2.091	+
koumine	2	3.46	−4.49	0.58	−3.275	1459.776	823.766	−3.034	0.711	100	0	+	+	1.576	-
vincanidine	1	1.874	−3.659	0.342	−5.307	170.798	81.028	−2.263	−0.078	77.877	0	+	-	3.348	-
myricetin	−2	−0.299	−5.008	−0.489	−6.439	6.527	2.149	−2.672	−2.948	26.816	1	+	+	1.98	-
gardnutine	2	3.145	−5.282	0.493	−3.818	952.247	519.112	−3.758	0.501	100	0	+	+	2.228	-
tabersonine	1	4.182	−5.604	0.866	−3.764	674.31	357.476	−4.404	0.297	100	0	+	-	3.452	-
isocorydine	1	3.298	−5.13	0.417	−3.518	1103.801	608.961	−3.46	0.383	100	0	+	+	2.537	-
oxoglaucine	0	2.931	−4.627	−0.122	−1.763	2282.141	1206.912	−3.402	−0.284	100	0	+	+	2.208	-
protopine	2	1.708	−4.379	−0.423	−3.551	1241.791	691.648	−1.129	0.714	92.322	0	+	-	1.634	-
chlorogenic acid	−2	−0.228	−3.277	−0.913	−6.184	1.725	0.649	−2.526	−3.313	16.89	1	+	-	1.835	-
cryptopine	2	2.45	−4.954	−0.158	−3.495	1241.119	691.243	−2.164	0.566	96.662	0	+	-	1.808	-
ethylrhoeagenine	2	2.05	−4.962	−0.508	−2.882	2407.669	1414.786	−1.436	0.831	100	0	+	+	2.37	-
S,R-noscapine	1	1.909	−4.853	−0.431	−4.013	736.111	393.017	−1.744	0.287	89.434	0	+	+	1.797	-
epsilon-viniferin	−2	3.639	−6.72	0.639	−4.08	30.819	11.507	−5.706	−2.615	74.901	0	+	-	1.824	-

[a]CNS PERM: above −2 capable of penetration; QPlogP o/w: coefficient of octanol/water partition lipophilicity (forecast between −2 and 6.5); QPlogHERG: blockage of HERG K^+ channels (projected IC_{50} value greater than −5); QPlogKhsa: albumin binding to human serum (anticipated to range from −1.5 to 1.5); QPlogKp: predicted skin permeability (between −8 and −1 cm/s); QPPCaco: Caco-2 cells function as a model for the gut-blood barrier, as expected (permeability is low if it is less than 25 nm/s and high if it is greater than 500 nm/s); QPPMDCK: appearance of MDCK cell permeability in anticipation of passive transport across the blood-brain barrier (permeability is low if it is less than 25 nm/s and high if it is greater than 500 nm/s); QPlogS: predicted aqueous solubility (range from −6.5 to 0.5); QPlogBB: ratio of brain to blood partition coefficient (range expected between −3 and 1.2); HIA: human intestinal absorption; SS: skin sensitization.

https://doi.org/10.1021/acsomega.3c07655
ACS Omega 2024, 9, 3642−3668

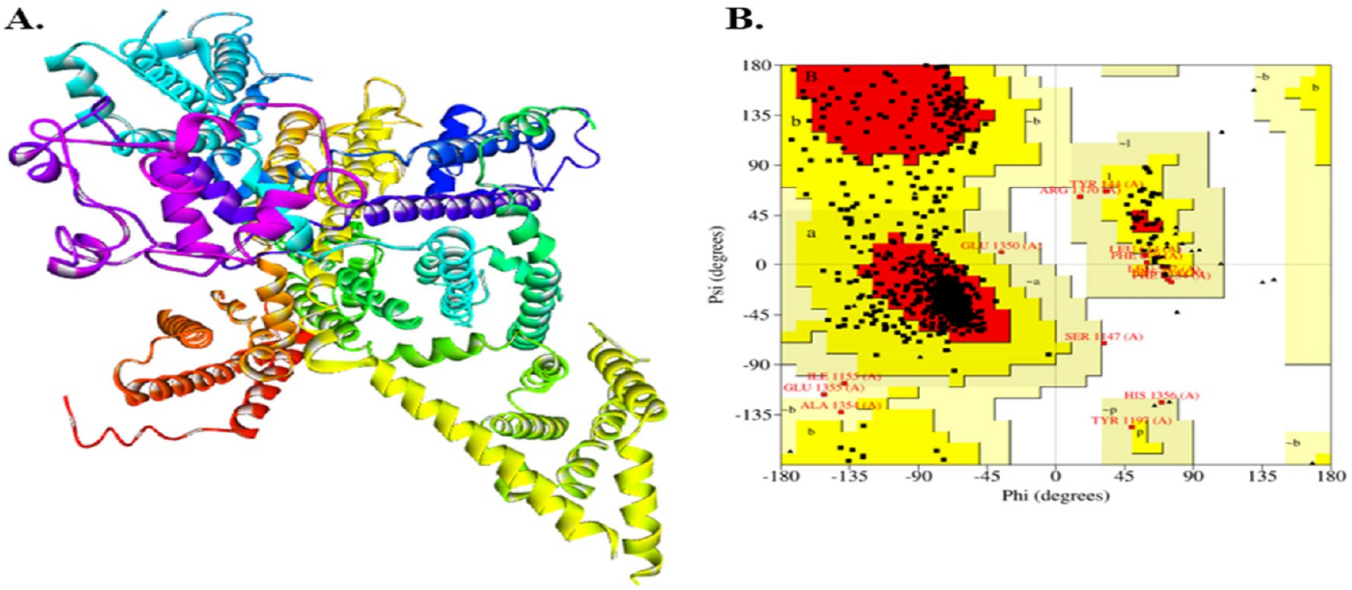

Figure 9. (A) Prepared CAC1C_ HUMAN (Q13936) protein model based on 8EOI and (B) Ramachandran plot Q13936 protein validation findings.

depicted in Tables 5 and 6. Using ADMETlab 2.0, SWISS ADME, Qikprop, and admetSAR, 33 bioactive compounds identified via LC-ESI-MS/MS analysis were evaluated for ADMET and drug-likeness to identify the following properties: number of rotatable bonds, GI absorption, H-bond acceptors, P glycoprotein substrate, the volume of distribution, topological polar surface area, bioavailability score, the CYP2D6, CYP2C9, and CYP3A4 metabolism, H-bond donors, total clearance, CNS permeability, half-life, HERG K^+ channels blockade, human serum albumin binding, skin permeability, gut blood barrier permeability, aqueous solubility, rule of five, partition coefficient octanol/water, human intestinal absorption, AMES mutagenesis, brain−blood barrier, acute oral toxicity (LD_{50}), and skin sensitization.

Various recovery profiles were seen for each compound. All compounds displayed favorable pharmacokinetic features and no significant side effects, indicating their potential therapeutic use. Therefore, ADMET analysis enabled the identification of ligands with important pharmacokinetic features within acceptable limits.

Each of the isolated bioactive compounds exhibited water solubility, human serum albumin affinity, and lipophilicity partition coefficient within the acceptable range; bioavailability, metabolism, CNS permeability, excretion, and distribution volume were all adequate; high GI absorption except for bergenin, (methylsulfanyl) butyl glucosinolate, myricetin, and chlorogenic acid, which can be modified during formulation development; and epsilon-Viniferin was outside the acceptable range of HERG K+ channel blockage. These factors all contribute to the proper internal distribution of ligands.

The rule of five analysis established by Lipinski rejected myricetin and chlorogenic acid; AMES mutagenesis investigations identified koumidine, bergenin, hydrocotarnine, ellipticine, 2′,5-dimethoxyflavone, koumine, myricetin, gardnutine, isocorydine, oxoglaucine, ethylrhoeagenine, and S, R-noscapine as positive; therefore, these compounds did not fall under the permissible limit. Serotonin was an amino acid molecule that was excluded from in silico research. After screening the 33 compounds with in silico drug-likeness and ADMET prediction, only 19 bioactive compounds remained for network pharmacology study.

2.4.2. Modeling Protein Homology. Voltage-dependent L-type calcium channel subunit alpha-1C protein (Q13936: CAC1C_ HUMAN) homology model was constructed using sequence data from UniProtKB.

2.4.2.1. Physicochemical Characteristics. Physicochemical properties of CAC1C_HUMAN sequencing data were investigated using the ProtParam tool web service. The amino acid profile of CAC1C_ HUMAN revealed amino acids 2221 with a total molecular weight of 248976.62 and maximal Leu (L) 227 (10.2%), Ala (A) 171 (7.7%), and Ser (S) 159 (7.2%) residues with 240 Asp + Glu (negatively charged) and 225 Arg + Lys (positively charged) residues. The elevated aliphatic index of the protein, 92.53, demonstrated its exceptional thermostability, although a −0.052 GRAVY score showed a larger possibility of water and protein interacting efficiently. The protein's pI was 6.33, suggesting its acidity, while its instability index was 48.87, indicating its instability. This instability was anticipated due to the dipeptide manifestation, often absent in protein stability. 244,660 (M^{-1} cm^{-1}) was the extinction coefficient at 280 nm in water, while 0.983 resulted from 0.1% (=1 g/L) abs, supposing that every pairing of Cys residues produces cystines. In a solution, this metric assesses the interactions between protein−protein and protein−ligand.

2.4.2.2. Validation of Homology Modeling. Figure 9A illustrates the prepared CAC1C_ HUMAN (Q13936) protein model based on the 8EOI, and Figure S3 depicts the secondary structure sequence alignment of the 8EOI. The PROCHECK was used to check the model. In addition, the Ramachandran plot revealed the amino acid distribution as phi and psi degrees and validated the Q13936 model. The structure was determined using the estimated values. CAC1C_ HUMAN (Q13936) protein's amino acid residues comprised 83.2% of the most preferred areas and 0.2% of the prohibited regions (Figure 9B). When adequately aligned and finished, a model with low sequence similarity may be ideal for molecular docking research.

2.4.3. Network Pharmacology Analysis. 2.4.3.1. Prospective Target Evaluation. Swiss target prediction and DrugBank databases were queried to identify possible protein targets for

https://doi.org/10.1021/acsomega.3c07655
ACS Omega 2024, 9, 3642−3668

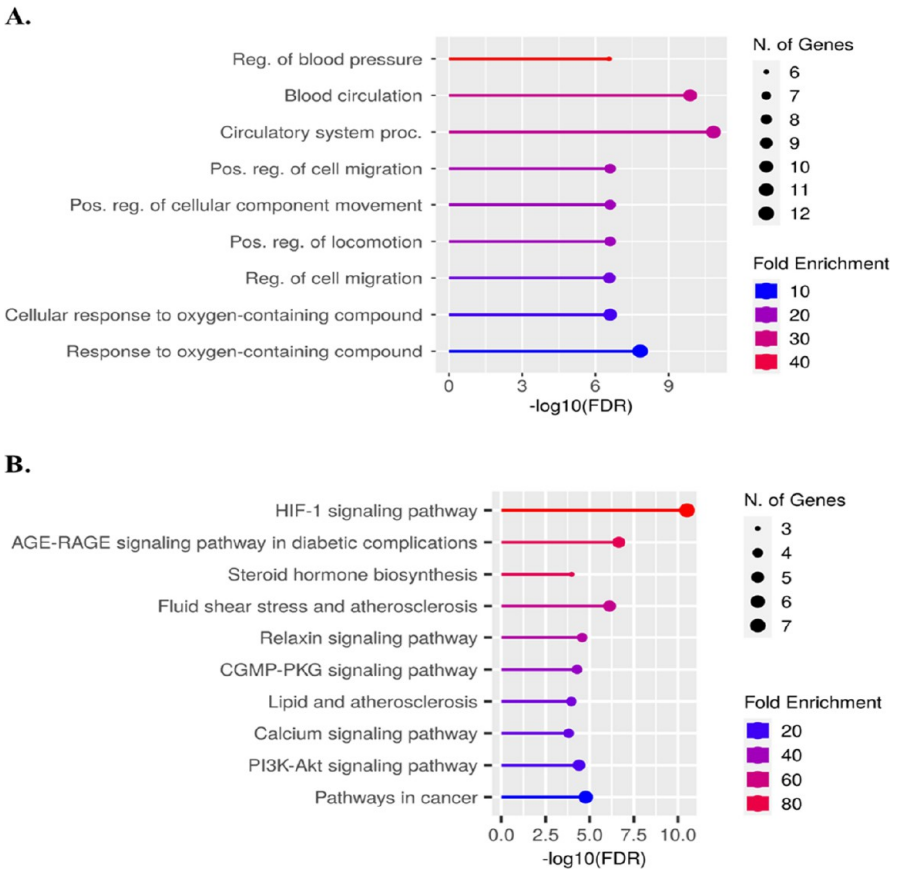

Figure 10. Functional enrichment utilizing (A) Gene Ontology (GO) and (B) Kyoto Encyclopedia of Genes and Genomes (KEGG) was depicted, displaying the top ten enriched terms based on the number of genes and fold enrichment.

the remaining 19 bioactive components in the *Fumaria indica* (Hausskn.) Pugsley hydromethanolic extract.

Due to the absence of data in the databases, as mentioned above, hulupinic acid was excluded from the network pharmacology investigation. Umbelliferone failed to intersect with target genes after using a 0.03 probability-based cutoff threshold. Tables S1 and S2 represent the top 150 pathogenic target genes for hypertension analyzed via VarElect and bioactive compounds' most likely macromolecular targets, respectively. In Figure S4, a Venn diagram depicts the relationship between hypertension-related genes and bioactive chemical targets. Consequently, 15 putative hypertension disease target genes overlap. These overlapping targets were utilized for GO and KEGG pathway research and network construction.

2.4.3.2. GO and KEGG Evaluation. The GO biological process for *Fumaria indica* (Hausskn.) Pugsley hydromethanolic extract demonstrated a prevalence of hypertensive target genes for bioactive compounds, emphasizing reg. of blood pressure and cell migration, blood circulation, circulatory system proc., pos. reg. of locomotion, cell migration, and cellular component movement, cellular response, and response to oxygen-containing compounds (Figure 10A and Table S3). The KEGG enrichment evaluation revealed a predominance of hypertension-target genes for bioactive compounds, with emphasis on the following signaling pathways: calcium, fluid shear stress and atherosclerosis, steroid hormone biosynthesis, relaxin, lipid and atherosclerosis, CGMP-PKG, HIF-1, AGE-RAGE in diabetic complications, PI3K-Akt, and pathways in cancer (Figure 10B and Table S4).

2.4.3.3. Network Construction. The protein−protein Interaction (PPI) STRING network for hypertension disease target genes had 15 nodes and 38 edges (Figure 11A). Cytoscape developed a CTD network of 25 nodes and 15 edges between putative hypertension disease target genes and bioactive chemicals from FIP (Figure 11B and Table S5). The CTP network of GO biological processes for FIP bioactive compounds consisted of 33 nodes and 96 edges for hypertension disease target genes (Figure 11C and Table S6). The CTP network of KEGG pathways for FIP bioactive compounds comprised 35 nodes and 62 edges for hypertension disease target genes (Figure 11D and Table S7).

2.4.3.4. Target Analysis and Pathway Evaluation. The MCODE cluster network of Fip.Cr hub proteins are illustrated in Figure 11E. Fip.Cr hub proteins implicated in the therapy of hypertension might include MMP9, JAK2, HMOX1, NOS2, NOS3, TEK, SERPINE1, CCL2, and VEGFA. Table 7 illustrates the KEGG pathways of FIP hub genes associated with hypertension therapy.

2.4.4. Molecular Docking. Molecular docking calculations estimated the ligand location in the target protein binding pocket. Physical factors, including solvation energy, are merged with a unified force field for precise docking calculation. Table 8 and Figure S5 both depict the results.

2.4.4.1. CAC1C_ HUMAN. The greatest docking score was achieved by (methylsulfanyl) butyl glucosinolate (docking score: −6.93 kcal/mol, glide energy: −46.79, ΔG binding: −41.93 kcal/mol, pK_i: −14.98 μM), which interacted with TYR144 (2.13 Å), TYR144 (2.51 Å), GLN671 (2.34 Å), ASP150 (1.80 Å), PHE147 (1.97 Å) to produce conventional H-

https://doi.org/10.1021/acsomega.3c07655
ACS Omega 2024, 9, 3642−3668

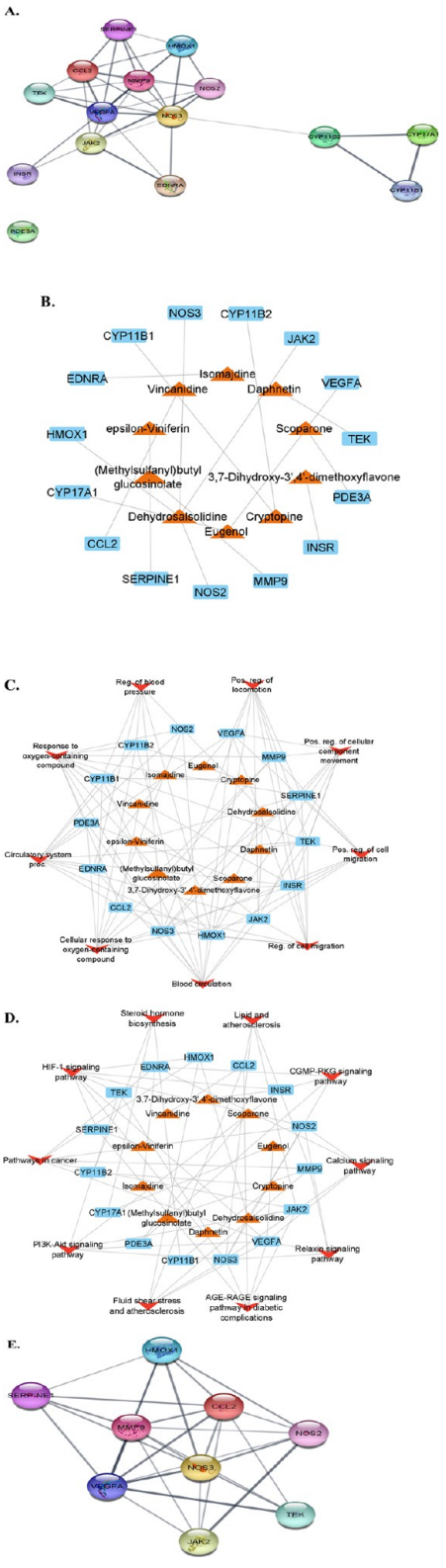

Figure 11. (A) PPI STRING network of hypertension; (B) CTD network of bioactive compounds with hypertension disease target genes; CTP networks of (C) GO biological processes and (D) KEGG pathways of bioactive compounds with hypertension disease target genes; (E) Fip.Cr hub proteins and MCODE cluster network. Note. Interactive Fip.Cr key targets in hypertension therapy. PPI: Protein−protein Interaction; CTD: Compounds Targets Disease; and CTP: Compounds Targets Pathways.

Table 7. KEGG Pathways of FIP Hub Genes Associated with Hypertension Therapy

sr. no.	term	description	gene symbols
1	hsa04020	calcium signaling pathway	**NOS2,** HEP-NOS, INOS, NOS, NOS2A
2	hsa04630	JAK-STAT signaling pathway	**JAK2,** JTK10
3	hsa04060	cytokine-cytokine receptor interaction	**CCL2,** GDCF-2, HC11, HSMCR30, MCAF, MCP-1, MCP1, SCYA2, SMC−CF
4	hsa04066	HIF-1 signaling pathway	**SERPINE1,** PAI, PAI-1, PAI1, PLANH1
5	hsa04926	relaxin signaling pathway	**MMP9,** CLG4B, GELB, MANDP2, MMP-9
6	hsa04151	PI3K-Akt signaling pathway	**NOS3,** ECNOS, eNOS
7	hsa04370	VEGF signaling pathway	**VEGFA,** MVCD1, VEGF, VPF
8	hsa05418	fluid shear stress and atherosclerosis	**HMOX1,** HMOX1D, HO-1, HSP32, bK286B10
9	hsa04014	ras signaling pathway	**TEK,** CD202B, GLC3E, TIE-2, TIE2, VMCM, VMCM1

bonds; and with PRO146 (5.37 Å) resulted in alkyl interaction. The ranked second in docking score was epsilon-viniferin (docking score: −5.13 kcal/mol, glide energy: −53.47, ΔG binding: −40.01 kcal/mol, pK_i: −14.15 μM Å), interatomic contacted with GLU149 (1.59 Å), GLN671 (1.65 Å), PRO148 (1.92 Å), ASN156 (1.80 Å) to produce conventional hydrogen bond; with GLY674 (2.45 Å) to form a carbon−hydrogen bond, and with LYS234 (4.20 Å) resulted in pi-alkyl interaction. The ranked third in docking score was eugenol (docking score: −5.12 kcal/mol, ΔG binding: −30.79 kcal/mol, glide energy: −22.58, pK_i: −10.14 μM), which interacted with TYR144 (1.59 Å) to produce conventional hydrogen bond; with GLN671 (2.93 Å), GLN671 (2.79 Å) to form carbon−hydrogen bond; with LEU141 (3.83 Å), ARG240 (4.48 Å), VAL241 (4.45 Å) resulted in alkyl interaction; and with TYR144 (5.18 Å), MET670 (4.27 Å) to create pi-Alkyl interaction. Scoparone (docking score: −4.87 kcal/mol, ΔG binding: −33.21 kcal/mol, glide energy: −25.93, pK_i: −11.20 μM) interacted with ASP150 (1.91 Å) to produce conventional hydrogen bond; with ASP150 (2.97 Å), GLY674 (2.61 Å), MET670 (2.55 Å), GLN671 (2.97 Å), PHE673 (2.47 Å), PHE673 (2.84 Å) to form carbon−-hydrogen bond; with PRO146 (4.43 Å), MET670 (4.57 Å) to create alkyl interaction; and with TYR144 (5.30 Å), PRO146 (5.27 Å) resulted in pi-alkyl interaction. Sinapic acid (docking score: −4.77 kcal/mol, ΔG binding: −12.86 kcal/mol, glide energy: −22.70, pK_i: −2.36 μM) interatomic contacted with ASP150 (1.88 Å) to form conventional hydrogen bond; with GLU149 (2.98 Å), ASP150 (2.40 Å), ASP151 (2.40 Å) to create carbon−hydrogen bond; with LYS234 (4.47 Å) resulted in alkyl interaction; and with PHE147 (4.66 Å) resulted in pi-alkyl interaction. 2-Coumaric acid (docking score: −4.01 kcal/mol, ΔG binding: −14.20 kcal/mol, glide energy: −14.61, pK_i: −2.94 μM) interacted with TYR144 (1.87 Å), GLN671 (2.21 Å), GLN671 (1.85 Å) to produce conventional hydrogen bond; and with ARG237 (2.87 Å) to form carbon−hydrogen bond. Dehydrosalsolidine (docking score: −4.01 kcal/mol, ΔG binding: −30.50 kcal/mol, glide energy: −28.29, pK_i: −10.02 μM) interacted with ASP150 (2.22 Å), GLN671 (1.94 Å) to produce conventional hydrogen bond; with ASN156 (2.68 Å), ASP150 (2.59 Å), GLU149 (2.56 Å) to form a carbon−-hydrogen bond; with PRO146 (5.34 Å) resulted in alkyl

https://doi.org/10.1021/acsomega.3c07655
ACS Omega 2024, 9, 3642−3668

Table 8. Prime MMGBSA Binding Energy (kcal/mol) Estimations for Compounds with the Voltage-Dependent L-type Calcium Channel Alpha-1C Subunit (CAC1C_HUMAN)[a]

sr. no.	compound	docking score	$\Delta G_{binding}$	glide energy	log K_i (μM)	$\Delta G_{solv\ GB}$	ΔG_{Hbond}	ΔG_{vdW}	$\Delta G_{coulomb}$	$\Delta G_{lipophilic}$	$\Delta G_{covalent}$	ligand-residue interactions with distance (Å)	
												hydrogen bond	electrostatic/ hydrophobic
1	(methylsulfanyl) butyl glucosinolate	−6.93	−41.93	−46.79	−14.98	22.75	−4.10	−37.55	−16.54	−9.05	2.56	**salt bridge:** LYS676 (2.23); **conventional hydrogen bond:** TYR144 (2.13), TYR144 (2.51), GLN671 (2.34), ASP150 (1.80), PHE147 (1.97)	**attractive charge:** LYS676 (2.23); **alkyl:** PRO146 (5.37)
2	epsilon-viniferin	−5.13	−40.01	−53.47	−14.15	40.63	−3.08	−36.93	−34.94	−12.19	8.59	**conventional hydrogen bond:** GLU149 (1.59), GLN671 (1.65), PRO148 (1.92), ASN156 (1.80); **carbon hydrogen bond:** GLY674 (2.45)	**pi-cation:** LYS676 (4.29); **pi-anion:** GLU149 (3.84); **pi-pi stacked:** TYR144 (5.44); **pi-alkyl:** LYS234 (4.20)
3	eugenol	−5.12	−30.79	−22.58	−10.14	10.31	−0.55	−19.94	−6.20	−19.46	6.11	**conventional hydrogen bond:** TYR144 (1.59); **carbon hydrogen bond:** GLN671 (2.93), GLN671 (2.79)	**pi-pi T-shaped:** TYR144 (4.82); **alkyl:** LEU141 (3.83), ARG240 (4.48), VAL241 (4.45); **pi-alkyl:** TYR144 (5.18), MET670 (4.27)
4	scoparone	−4.87	−33.21	−25.93	−11.20	12.36	−0.67	−27.89	−4.38	−11.65	0.75	**conventional hydrogen bond:** ASP150 (1.91); **carbon hydrogen bond:** ASP150 (2.97), GLY674 (2.61), MET670 (2.55), GLN671 (2.97), PHE673 (2.47), PHE673 (2.84); **pi-donor hydrogen bond:** PHE147 (2.92)	**alkyl:** PRO146 (4.43), MET670 (4.57); **pi-alkyl:** TYR144 (5.30), PRO146 (5.27)
5	sinapic acid	−4.77	−12.86	−22.70	−2.36	5.19	−2.23	−23.53	12.35	−7.45	3.21	**salt bridge:** ARG237 (1.81), ARG237 (3.17); **conventional hydrogen bond:** ASP150 (1.88); **carbon hydrogen bond:** GLU149 (2.98), ASP150 (2.40), ASP151 (2.40)	**attractive charge:** ARG237 (1.81), ARG237 (3.17), ARG240 (5.30); **pi-anion:** ASP150 (3.54); **alkyl:** LYS234 (4.47); **Pi-alkyl:** PHE147 (4.66)
6	2-coumaric acid	−4.01	−14.20	−14.61	−2.94	−5.19	−1.56	−14.72	18.22	−12.94	3.74	**conventional hydrogen bond:** TYR144 (1.87), GLN671 (2.21), GLN671 (1.85); **carbon hydrogen bond:** ARG237 (2.87)	**attractive charge:** ARG240 (5.52); **pi-sulfur:** MET670 (5.40)
7	dehydrosalsolidine	−4.01	−30.50	−28.29	−10.02	15.30	−1.14	−25.55	−11.31	−9.65	1.89	**conventional hydrogen bond:** ASP150 (2.22), GLN671 (1.94); **carbon hydrogen bond:** ASN156 (2.68), ASP150 (2.59), GLU149 (2.56)	**alkyl:** PRO146 (5.34); **pi-alkyl:** PHE147 (5.22)
8	verapamil	−3.84	−37.17	−45.42	−12.91	35.19	−1.50	−40.25	−19.05	−14.41	3.89	**salt bridge:** GLU149 (1.76); **conventional hydrogen bond:** PHE147 (2.14), PHE147 (2.83); **carbon hydrogen bond:** PRO146 (2.74), GLU149 (2.26), PHE147 (2.63), ILE145 (2.46), ASN156 (2.57), ASN156 (2.63)	**attractive charge:** GLU149 (1.76), ASP150 (5.51); **pi-cation:** LYS676 (4.37); **pi-pi T-shaped:** TYR719 (5.73); **alkyl:** LEU728 (5.24), VAL729 (4.83), PRO146 (4.92); **pi-alkyl:** TYR144 (4.17), TYR719 (4.73)

[a]ΔG Binding: binding free energy; pK_i: logarithmic of inhibition constant K_i; ΔG bind solv GB: generalized born electrostatic solvation energy; ΔG bind H bond: hydrogen bonding energy; ΔG bind vdW: van der Waals forces energy; ΔG bind coulomb: coulomb binding energy; ΔG bind lipophilic: lipophilic binding energy; ΔG bind covalent: covalent binding energy; These energies all contribute to ΔG binding, the free energy of binding.

https://doi.org/10.1021/acsomega.3c07655
ACS Omega 2024, 9, 3642−3668

interaction; and with PHE147 (5.22 Å) resulted in pi-alkyl interaction.

Verapamil (docking score: −3.84 kcal/mol, ΔG binding: −37.17 kcal/mol, glide energy: −45.42, pK_i: −12.91 μM) interacted with PHE147 (2.14 Å), PHE147 (2.83 Å) to produce conventional hydrogen bond; with PRO146 (2.74 Å), GLU149 (2.26 Å), PHE147 (2.63 Å), ILE145 (2.46 Å), ASN156 (2.57 Å), ASN156 (2.63 Å) to form carbon−hydrogen bond; with LEU728 (5.24 Å), VAL729 (4.83 Å), PRO146 (4.92 Å) resulted in alkyl interaction; and with TYR144 (4.17 Å), TYR719 (4.73 Å) resulted in pi-alkyl interaction.

3. DISCUSSION

Substantial evidence supports the traditional use of *Fumaria indica* (Hausskn.) Pugsley as a treatment for various ailments and its remarkable therapeutic advantages. Consequently, this study aimed to establish the veracity of *Fumaria indica*'s folkloric claims for the treatment of hypertension by investigating its mechanism of action, exploring the cardioprotective potential, identifying bioactive compounds, and assessing its toxicity.

The LC−MS/MS analysis of *Fumaria indica* (Hausskn.) Pugsley hydromethanolic extract revealed the predominant presence of alkaloids, coumarins, phenylpropanoids, flavonoids, and other identified chemicals were sinapic acid, bergenin, (methylsulfanyl)butyl glucosinolate, p-coumaraldehyde, dehydrosalsolidine, hydrocotarnine, ellipticine, hulupinic acid, isocorydine, koumine, serotonin, and linoleic acid. The previous phytochemical research indicated comparable results.[44−46]

Fip.Cr was evaluated for potential vasorelaxant effects on endothelium-intact and endothelium-denuded aortic tissue preparations. Fip.Cr exerted a vasorelaxant effect on both preparations. Experiments on vascular preparations revealed that Fip.Cr cumulative addition relaxed K^+ (80 mM) induced contractions at 1.0 mg/mL concentration. K^+ (80 mM) induces depolarization by augmenting the release of intracellular Ca^{2+} through voltage-dependent Ca^{2+} channels.[47]

Calcium channel blockade may assist the vasorelaxant effect of the Fip.Cr, as evidenced by its capacity to alleviate K^+ (80 mM) precontraction because smooth muscle relaxation will occur following repolarization by preventing the inflow of calcium current.[48] After testing Fip.Cr on a vascular preparation that had been precontracted with phenylephrine, we discovered that it generated full relaxation at the same concentration and that the nitric oxide synthase inhibitor L-NAME[49] had no impact on this relaxation, thereby excluding the involvement of nitric oxide pathway. PE stimulates α-adrenergic receptors, creating inositol-1,4,5-triphosphate via the conversion of phosphatidylinositol, activating voltage-dependent calcium channels to raise intracellular calcium.[50]

Consequently, similarly to verapamil, Fip.Cr exhibited a relaxant response to K^+ (80 mM) and phenylephrine (1 μM) induced contractions, representing a blockade of intracellular calcium influx via calcium channels. Essential to the treatment of hypertension and angina are medications that block calcium channel function.[51]

Fip.Cr was further evaluated on isolated rat atrial strips to get insight into its effects on cardiac muscles. Fip.Cr completely blocked the rate (negative chronotropic) and force (negative inotropic) of atrial spontaneous contractions, comparable to verapamil. The inotropic and chronotropic hypotensive effects were unaffected by atropine pretreatment, ruling out a role for muscarinic receptors in the heart. Electrical stimulation of cardiac myocytes initiates heart muscle contraction (excitation and contraction coupling, ECC).[52] The most plausible explanation for these results is that Fip.Cr may be manifested via calcium ion channel blockade as a hypotensive mechanism.

To ensure plant products' safety, conducting exhaustive studies of their toxicity is vital, offering scientific evidence for determining acceptable doses for animals, including humans.[53] Acute toxicity is a preliminary investigation that is the foundation for categorization and labeling. In addition, it gives preliminary information regarding the method of toxic action of a chemical, allowing us to determine the dose of a novel molecule and assisting in animal research dose determination.[54,55] Our investigations revealed that acute toxicity from a single dosage of escalating Fip.Cr did not result in any mortality or significant abnormalities at any level. However, a moderate sedative effect was seen in rats at 2000 mg/kg, b.wt. dose. The study's limit test dose was 2000 mg/kg b.w., which did not demonstrate significant toxicity and fatality; therefore, subacute toxicity tests were performed with doses (500, 250, and 125 in mg/kg, b.wt.) that were a quarter, an eighth, and a 16th of the limit test dosage, respectively.

In rats, subacute administration of Fip.Cr did not result in any behavioral abnormalities or mortality. Initial warning indications of toxicity from chemicals and medications manifest in changes in general behavior and body weight.[56] Compared to the control group, the rise in rat body weight was insignificant and deemed normal. Consequently, it can be inferred from the acute and subacute toxicity investigations that oral administration of Fip.Cr did not cause significant clinical symptoms or alter the normal development pattern of rats.

Rats' kidneys, lungs, stomach, intestines, spleen, liver, pancreas, and heart were analyzed for any discernible morphological differences. A comprehensive evaluation of the vital organs of the rats found no abnormalities or degeneration. When assessing the toxicity of a product, drug, or chemical, relative organ weight is a good indicator and reliable predictor of toxicity. Our investigation indicated that after administering Fip.Cr at varying dosages to rats, all organ modifications were insignificant; hence, it can be inferred that administration of Fip.Cr at varying doses did not produce any major complications to the vital organs.

The hematopoietic system, one of the most susceptible bodily systems to the impacts of toxic compounds, is also a good indication of human and animal pathological and physiological status.[57] An examination of hematological parameters, which may also be used to explain the blood-related activities of extracts, can indicate the potentially harmful effects of an extract on an animal's blood.[58,59] Rats' hepatic and renal functions were analyzed using clinical biochemistry to determine whether or not the extract had any effect. The liver and kidney are essential for an organism's survival, so the biochemical parameters are considered a crucial toxicity assessment signal.[60] The hematological and biochemical profile of rats treated with Fip.Cr was mostly nonsignificant compared to the control group and was within the usual range. These findings demonstrated that acute and subacute treatment of Fip.Cr did not significantly affect the hematological and biochemical profile of rats, nor did it cause noteworthy harmful repercussions.

Histopathological slides allow for a more in-depth investigation of toxic effects and ailments since the tissue architecture is preserved throughout fabrication.[61] Compared to the normal control group, histological examinations of the heart, liver, kidneys, and lungs revealed no significant alterations. These results were compatible with hematological and biochemical

https://doi.org/10.1021/acsomega.3c07655
ACS Omega 2024, 9, 3642−3668

measures that showed no substantial changes. Since no detrimental effects on the hematopoietic system are observed, these results might indicate the extract's safety at up to 2000 mg/kg.[62]

Experimental results on the aorta and atrial preparations revealed that Fip.Cr might have hypotensive effects on anesthetized rats with normotensive blood pressure. The Fip.Cr exerted hypotensive effects on anesthetized rats, with comparable decreases in mean arterial (MABP), systolic (SBP), and diastolic (DBP) blood pressure to those observed with verapamil. These findings demonstrated that the voltage-dependent calcium channel-blocking activity might play a crucial role in the antihypertensive potential of Fip.Cr.

After exposing rats to isoproterenol (ISO)-induced myocardial infarction, we determined that Fip.Cr exhibited cardioprotective properties. ISO is a synthetic, nonselective beta-adrenergic agonist, and ISO-induced myocardial damage has frequently been used in pharmacological investigations to examine the effect of drugs on myocardial infarction.[63,64] Elevated biometrical indicators, serum levels of CPK, CK-MB, lipid profile, LDH, cTnT, ANP, AST, ALT, and serum IL-6, as well as abnormal cardiac microstructure on histopathology in the ISO administered group, indicate that the current research is an efficient rat model of myocardial injury. These findings are consistent with prior *in vivo* investigations.[65,66] Consequently, the current study confirmed that Fip.Cr could ameliorate ISO-induced myocardial infarction injury, as evidenced by a significant decrease in biometrical indicators, serum levels of myocardial injury markers, and a marked reduction in histopathological alterations comparable to carvedilol and verapamil.

Oxidative stress-induced inflammation of cells includes the inflammasome containing the NOD-like receptor pyrin superfamily domain 3 (NLRP3).[67] This inflammasome protein complex includes ASC, NLRP3, and caspase-1 as constituents. Patients with acute myocardial infarction have peripheral blood monocytes that are NLRP3 inflammasome-activated. Furthermore, it has been observed that treatment of NLRP3 siRNA plus BAY 11-7082, an inflammasome inhibitor, greatly improved myocardial *ischemia/reperfusion injury*.[68,69,70] Myocardial infarction (MI) damage is also influenced by tumor necrosis factor- α (TNF- α), IL-1β, and IL-6. TNF- α antagonists perform a therapeutic function in MI.[71] These data suggest that NLRP3 inflammasome, TNF- α, IL-1β, and IL-6 have a role in myocardial infarction damage. In the current work, we demonstrated that ISO-induced myocardial injury activated NLRP3 inflammasome in the heart, as determined by increased cardiac expression levels of ASC, NLRP3, and caspase-1; and TNF-α, IL-1β, and IL-6 expression levels were also elevated. Our findings revealed that Fip.Cr, like carvedilol and verapamil, decreased NLRP3 inflammasome activation and TNF-α, IL-1β, and IL-6 levels, which are prospective therapeutic targets for the treatment of myocardial infarction damage.

Cardiovascular disorders are associated with an abnormal gut microbiome.[72] AMI patients' gut microbiota contained a decreased proportion of the phylum Firmicutes.[73] By enhancing cardiac pump performance in AMI patients, Lactobacillus may minimize the incidence of severe outcomes such as HF.[74] In the present investigation, the administration of ISO lowered the abundance of Firmicutes and Lactobacillus. The Fip.Cr affected the gut microbiome by increasing the abundance of Firmicutes and Lactobacillus compared to carvedilol and verapamil, demonstrating its cardioprotective potential. Previous investigations have revealed that alkaloids and flavonoids are cardioprotective.[75] Consequently, the bioactive compounds identified in the current investigation may be accountable for Fip.Cr's cardioprotective effect.

In 2007, Hopkins proposed network pharmacology to discover how ligands and drugs function within cells.[76] The generated networks of network pharmacology depict the interplay between many targets, bioactive chemicals, and the pathways of bioactive substances in herbal and complicated diseases.[77] Recently, network pharmacology has emerged as an innovative method for highlighting the bioactivity of herbs and elucidating cellular pathways.[78] The hypertension-treating mechanism of FIP may include MMP9, JAK2, HMOX1, NOS2, NOS3, TEK, SERPINE1, CCL2, and VEGFA, according to network pharmacology research in the current study. According to computational assessments, the bioactive components of FIP manifested to treat hypertension are implicated in the control of many major KEGG pathways, including the calcium signaling pathway.

Molecular docking has become essential to drug discovery.[79] Molecular docking studies demonstrated that (methylsulfanyl) butyl glucosinolate, epsilon-viniferin, eugenol, scoparone, sinapic acid, 2-coumaric acid, and dehydrosalsolidine have a greater affinity for the voltage-dependent calcium channel (CAC1C_ HUMAN) than verapamil. Consequently, it became plausible to hypothesize that the antihypertensive effect of the FIP was due to the high affinity of the identified compounds for the protein of voltage-dependent calcium channel targeted by smooth muscle, which might hinder contraction-related signal transmission.

4. CONCLUSIONS

It can be concluded that the alkaloids and flavonoids identified in Fip.Cr may be responsible for its hypotensive and cardioprotective effects. Fip.Cr dramatically mitigated the ISO-induced myocardial infarction damage by attenuating inflammation in rats via inhibiting the NLRP3 inflammasome and raising the levels of Firmicutes and Lactobacillus. In vitro and *in vivo* experiments demonstrated that the antihypertensive mechanism of Fip.Cr may involve calcium channel blocker activity. The network pharmacology investigation revealed that FIP bioactive compounds may interfere with the hypertension-related genes and KEGG pathways. MMP9, JAK2, HMOX1, NOS2, NOS3, TEK, SERPINE1, CCL2, and VEGFA may all have a role in the hypotensive mechanism of FIP. In addition, a molecular docking study demonstrated that FIP bioactive compounds, including (methylsulfanyl) butyl glucosinolate, epsilon-viniferin, eugenol, scoparone, sinapic acid, 2-coumaric acid, and dehydrosalsolidine exhibited a higher docking score with a voltage-dependent calcium channel protein (CAC1C_ HUMAN) than verapamil. The acute and subacute toxicity studies of Fip.Cr up to 2000 mg/kg on rats found no significant adverse effects. It has been demonstrated that the oral LD_{50} of Fip.Cr is larger than 2000 mg/kg, thus widely considered safe. Therefore, the current work provides a major mechanistic basis for compound identification, hypotensive mechanism and cardioprotective potential exploration, and a safety evaluation of Fip.Cr. However, more research is required to determine the precise mechanism by which Fip.Cr prevents the activation of the NLRP3 inflammasome in myocardial infraction-damaged heart tissue.

https://doi.org/10.1021/acsomega.3c07655
ACS Omega 2024, 9, 3642−3668

5. METHODS

5.1. Plant Material Conglomeration and Crude Extract Preparation. *Fumaria indica* (Hausskn.) Pugsley whole plant was conglomerated in February 2020 from wheat fields and alongside railway tracks in Multan, Pakistan. A professor from Bahauddin Zakariya University in Multan, Pakistan, named Dr. Zafar-Ullah Zafar, verified the specimen's validity (Voucher number: www.theplantlist.org/tpl1.1/record/kew-2815398), and a specimen was placed in the same institution's herbarium. Cleaning, shade drying, and milling the plant material resulted in a fine powder. One kilogram of plant powder was steeped in 70% aqueous methanol for 1 week at 25 °C in an amber-colored glass jar with an open cover and frequent shaking. The percolate was concurrently filtered with muslin via a filtering media, namely, paper (Whatman no. 1). Following three rounds of maceration, all filtrates were mixed. A rotary evaporator (Labtechnik AG, BUCHI 9230 Model, Switzerland) evaporated the organic solvent entirely under decreased pressure and 37 °C. An extract (Fip.Cr) of a dark brown, semisolid substance with a yield of about 7.5% was produced. Fip.Cr was dissolved in 10% DMSO in preparation for the *in vitro*experimentation.

5.2. Chemicals. In all studies, analytical research-grade chemicals and reagents were used. The following chemicals were obtained from St. Louis, Missouri, United States, Sigma Chemical Company, MO: atropine sulfate, acetylcholine chloride (ACh), phenylephrine hydrochloride (PE), and verapamil hydrochloride (KCl). Sodium chloride (NaCl) was obtained from Poole, United Kingdom's BDH Laboratory Supplies. Calcium chloride ($CaCl_2$), magnesium sulfate ($MgSO_4$), potassium dihydrogen phosphate (KH_2PO_4), sodium bicarbonate ($NaHCO_3$), and glucose ($C_6H_{12}O_6$) were purchased from Darmstadt, Germany, Merck. For research, China's heparin and Global Pharmaceuticals' ketarol 500 mg/mL (ketamine) were utilized. On the day of the experiment, dilutions and physiological salt solutions were freshly produced in distilled water/saline. In studies serving as controls, the solubilization vehicle had no impact.

5.3. LC ESI-MS/MS Analysis. Identification of potentially bioactive compounds of *Fumaria indica* (Hausskn.) Pugsley hydromethanolic extract was evaluated using a Linear Ion Trap Mass Spectrometer (United States − Thermo Scientific) connected to a source of electrospray ionization (LTQ XL Model).[80,81] Ultrasonic dissolution of plant extract Fip.Cr (20 mg/mL) in the methanol of LC−MS grade for 5 min at 25 °C, followed by 10 min of 12,000 rpm centrifugation, produced the sample solution. The supernatant was filtered using a filter nylon syringe 0.45 μm after collection. Methanol was used to dilute each approximately 50 μL sample stock solution until the final volume was 1 mL. This solution was injected directly by a syringe pump into the ESI interface using a 7.5 μL/min flow rate. The following are the optimal operational parameters of negative and positive ESI/MS ion spectroscopy: N2 auxiliary and sheath gas flow rates at 20 and 5.0 au, respectively; the capillary's temperature and voltage were set at 286 °C and 4.6 kV, respectively; and 50−2000 m/z range for mass scanning. Modifying collision-induced decomposition energy from 2 to 30 according to ionic parent molecule type enabled ESI-MS fragmentation. The ESI-MS/MS data were collected and interpreted using the software X-Calibur 2.0.7 by Thermo Scientific (Massachusetts City of Waltham, United States).[82]

5.3.1. Identification of Compounds. The bioactive compounds in the extract were identified by cross-referencing the mass spectra chromatogram with previously published reference libraries and data, such as the European Mass Bank (https://massbank.eu/MassBank/) and the North American Mass Bank (http://mona.fiehnlab.ucdavis.edu/).

5.4. Animals and Housing Conditions. The Department of Pharmacology ethics committee, BZU Multan, approved the procedures (reference number EC/06-PhDL/S2018), and the studies were conducted in strict conformity with the *Laboratory Animal Resources Commission*'s guidelines.[83] Rats of the Sprague−Dawley strain were provided by the same institution for practical reasons, weighing 170 ± 20 g, regardless of gender. The rats were housed in a facility that regulated temperature (22 ± 4 °C) and lighting with conventional food and unlimited tap water access.

5.5. Ethics Statement. All experiments were conducted following the Animals (Scientific Procedures) Act of the United Kingdom, enacted in 1986, and associated recommendations; ARRIVE guidelines; National Institutes of Health recommendations (1978 revision of NIH Publication Number 8040); or Directive 2010/63/EU for animal experimentation for the use and care of the laboratory animals.

5.6. In Vitro Tissue Experimentation. For *in vitro* experimentation, the approach outlined in previous studies[84−86] was utilized.

5.6.1. Vascular Investigations of Isolated Rat Aorta. Following a cervical dislocation, the rats' thoracic descending aortas were isolated and submerged in the carbogen-containing solution of Kreb. Without harming the aorta endothelium, all adhering fatty tissues were meticulously removed. Each (2−3 mm) preparation for an aortic ring was fixed in tissue organ baths of 15 mL containing carbogen accreted solution of Kreb and kept at 37 °C by a thermoregulator with circulation. Before drug testing, aortic ring preparations were subjected to 2 ± 0.1 g preloaded force, and after 10 ± 2 min, new Kreb's solution buffer drainage was permitted to stabilize for 55 ± 5 min. Using a FORT100 force−displacement transducer, the tissue's physiologic response was recorded. Lab Chart Pro Software Version 7 displayed the results of signal amplification achieved using Power Lab (4/25). Immediately before administering the test drug, the physiological activity was measured and quantified as a contraction percentage. After equilibration, the drug or test substances were delivered in sequence.

This research evaluated aorta preparations with intact and denuded endothelium in terms of nitric oxide and cholinergic-based (EDRF) relaxing factors produced from endothelium. Curved forceps were used to scrape the intima of the aortic ring to create an aortic preparation devoid of the endothelium. The ability of a bolus of acetylcholine (1 μM) administration to relax the constriction caused by phenylephrine (1 μM) validated the endothelial function. The endothelial activity was indicated by relaxing contraction of 70−80% (endothelium-intact). Contrary to this, additional contraction increases demonstrated endothelial dysfunction (endothelium-denuded).[87] Both aortic preparations were subjected to K^+ (80 mM) and phenylephrine (1 μM)-generated contractions in an organ tissue bath to investigate the potential vasorelaxant effect of Fip.Cr. L-NAME (10 μM) was utilized to assess the involvement of nitric oxide in the vasculature.

5.6.2. Mechanistic Basis of Isolated Rat Atria. Following a cervical dislocation, the rats' hearts were isolated and submerged in the carbogen-containing solution of Kreb. Ventricles and any adhering fatty tissues were meticulously removed without causing pacemaker damage. Atria's preparation was fixed in

https://doi.org/10.1021/acsomega.3c07655
ACS Omega 2024, 9, 3642−3668

tissue organ baths of 15 mL containing carbogen accreted solution of Kreb and kept at 37 °C by a thermoregulator with circulation. Before drug testing, atria's preparations were subjected to 1 ± 0.1 g preloaded force, and after 10 ± 2 min, new Kreb's solution buffer drainage was permitted to stabilize for 25 ± 5 min. Using a FORT100 force−displacement transducer, the tissue's physiologic response was recorded. Lab Chart Pro Software Version 7 displayed the results of signal amplification achieved using Power Lab (4/25). Immediately before administering the test drug, the physiological activity was measured and quantified as a contraction percentage. After equilibration, the drug or test substances were delivered in sequence.

5.7. In Vivo Tissue Experimentation. *5.7.1. Safety Assessment. 5.7.1.1. Acute Toxicity.* The acute toxicity experiments on Sprague−Dawley rats were done under OECD guideline 423, with minor adjustments. Four groups of five rats each were formed from the selected rats. Before the start of the experiment, each rat was weighed, marked for identifying purposes, and abstained from food during the night despite having access to water throughout.

1st group: The normal control group (NW) was administered a single dosage of 10 mL/kg bw of distilled water orally.

2nd group: The group treated with hydromethanolic extract (FAL) was administered a single dosage of 1000 mg/kg bw of Fip.Cr orally.

3rd group: The group treated with hydromethanolic extract (FAM) was administered a single dosage of 1500 mg/kg bw of Fip.Cr orally.

4th group: The group treated with hydromethanolic extract (FAH) was administered a single dosage of 2000 mg/kg bw of Fip.Cr orally.

Following dosing, the rats fasted for an additional 4 h, and continuous observations were obtained for every single rat in their separate groups for the first 4 h and twenty-four hours following the administration of drug therapy for mortality and aberrant alterations. Tremors, lethargy, diarrhea, respiration, sleep, aberrant behavior, drink and food intake, convulsions, changes in the skin, hair, and eye, color, salivation, motor activity, and coma were evaluated twice daily for 14 days to determine any toxicological effects. Acute toxicity was performed for informational purposes based on the test extract's short-term toxicity level, which assists in selecting the dosage for the repeated oral toxicity study.[88]

5.7.1.2. Subacute Toxicity. A 28-day investigation of the subacute toxicity of Fip.Cr in rats followed OECD standards 407.[89] Four groups of five rats each were constructed.

1st group: The normal control group (NW) administered a single dosage of 10 mL/kg bw distilled water orally.

2nd group: The group treated with hydromethanolic extract (FSL) was administered a single dosage of 125 mg/kg body weight of Fip.Cr orally.

3rd group: The group treated with hydromethanolic extract (FSM) was administered a single dosage of 250 mg/kg body weight of Fip.Cr orally.

4th group: The group treated with hydromethanolic extract (FSH) was administered a single dosage of 500 mg/kg body weight of Fip.Cr orally.

Throughout the research, all animals had unrestricted access to water and food until the day before their planned demise.[90,91]

5.7.1.3. Observations of Clinical and Survival. All of the animals were examined twice a day for death and disease. The clinical observation included alterations in the animal's skin, fur, mucous membrane, eyes, and autonomic activity, including pupil size, piloerection, abnormal breathing pattern, and lacrimation. Alterations in gait and posture were studied alongside stereotypical behaviors, including obsessive grooming and circling often. The observation lasted 1 week before test drug delivery until an autopsy was planned.

5.7.1.4. Body Weight. Throughout both studies, the weekly body weights of every animal were recorded. The body weights were also recorded both at the beginning of the study and at the end.

The correlation was used to determine the percentage gain in weight:

$$\text{gain in body weight (percent)} = (\text{last weight} - \text{original weight})/\text{original weight} \times 100$$

5.7.1.5. Necropsy and Organ Weight. All blood samples were collected on the final day of both investigations, and each animal fasted for a full night before the necropsy. After administering ketamine hydrochloride (100 mg/kg, intramuscularly), the animals were exsanguinated. The macroscopic examination comprised a review of the exterior surfaces, including the abdominal, thoracic, pelvic cavities, and cranial. The macroscopic characteristics of the kidneys, lungs, stomach, intestines, spleen, liver, pancreas, and heart removed during necropsy were observed. We cleansed the organs and deposited them in a 10% formalin solution that was neutrally buffered. These organs were also examined macroscopically for the likely development of lesions and other pathological indications.

Absolute (g) and relative weights (%) of organs were determined for the following important organs: the heart, kidney, liver, spleen, and lungs. The absolute weight of the essential organs was determined by removing them, placing them on absorbent sheets for a few minutes, and then weighing them (g). This approach determined the RW of each rat's respective organs:

$$\text{relative weight of organ (percent)} = (\text{ow (g)}/\text{bw on 29th day (g)}) \times 100$$

where ow = organ weight, bw = body weight, and RW = relative weight.

5.7.1.6. Hematological Analysis. The blood sample was stored in anticoagulant-containing sterile tubes, and the hematological profile was analyzed using an automated hematological analyzer (Sysmex XS-1000i). The following hematological parameters were examined: mean corpuscular volume, hemoglobin, and concentration of hemoglobin (MCV, MCH, and MCHC); red and white blood cells, and differential leucocyte counts (RBC, WBC, lymphocytes, neutrophils, monocytes, eosinophil); platelets, hematocrit (HCT), and hemoglobin (Hb %).

5.7.1.7. Biochemical Analysis. The serum was isolated from blood by centrifugation at 1500 × *g* for 15 min (no anticoagulant used). The recovered serum was refrigerated at −20 °C for future use. These biochemical parameters were assessed: glucose, bilirubin total, serum glutamic pyruvic transaminase (SGPT), urea, sodium, chloride, creatinine, potassium, alkaline phosphatase (ALP), total cholesterol, triglycerides, total protein,

https://doi.org/10.1021/acsomega.3c07655
ACS Omega 2024, 9, 3642−3668

Table 9. RT-PCR Primer Sequences

gene/targets	forward	reverse
ASC	5′-TTATGGAAGAGTCTGGAGCT-3′	5′-CAGCTGATGGACCTGACTGA-3′
NLRP3	5′-CAGCGATCAACAGGCGAGAC-3′	5′-AGAGATATCCCAGCAAACCTATCCA-3′
caspase-1	5′-CGTGGAGAGAAACAAGGAGTG-3′	5′-AATGAAAAGTGAGCCCCTGAC-3′
TNF-α	5′-CCCACTCTGACCCCTTTACT-3′	5′-TTTGAGTCCTTGATGGTGGT-3′
IL-1β	AGATGATAAGCCCACTCTACAG	ACATTCAGCACAGGACTCTC
IL-6	AGTTGCCTTCTTGGGACTGA	ACAGTGCATCATCGCTGTTC
GAPDH	5′-TTCAACGGCACAGTCAAGG-3′	5′-CACCAGTGGATGCAGGGAT-3′
V2	AgAgTTTgAgCCTgg CTC Ag	TgCTgC CTC CCg Tag gAg T
Firmicutes	GGCAGCAGTRGGGAATCTTC	ACAC[Y]TAG[Y]ACTCATCGTTT
Lactobacillus	CAT CCA GTG CAA ACC TAA GAG	GAT CCG CTT GCC TTC GCA

HDL cholesterol, serum glutamic oxaloacetic transaminase (SGOT), LDL cholesterol, and albumin. These values were determined using commercially available biochemistry analyzers and diagnostic test kits as evaluation tools.

5.7.1.8. Histopathological Studies. Histopathological studies were performed on organ samples of the heart, liver, kidneys, and lungs. The primary organs were surgically removed and preserved in a 10% formalin-buffering solution (pH 7.4).[92] Following fixation, tissue samples were dehydrated in a succession of ethanol concentrations ranging from 70 to 99.9%, rinsed with toluene, and then encased in paraffin. The tissue was sectioned to a thickness of 5 μm employing a rotary microtome, and then hematoxylin and eosin stained the slices (HE). The slices were then photomicrographed and examined microscopically for pathological diagnoses.[88]

5.7.2. Blood Pressure and Hemodynamic Parameters Assessment in Anesthetized Rats. Five mg/kg Diazepam and 85 mg/kg ketamine were administered intraperitoneally to 200−250g rats individually to achieve adequate anesthesia without affecting cardiovascular markers within the normotensive range. The rats were positioned supine on the dissection table, and an overhead lamp was used to maintain the temperature. An 18-gauge polyethylene tube was inserted into the trachea to facilitate breathing after a tracheotomy. The jugular vein of the right side was catheterized for intravenous drugs and Fip.Cr delivery. Fill heparinized saline (50 IU/mL) in polyethylene tubing while performing carotid artery cannulation to measure changes in hemodynamic parameters using an MLT 0699 pressure transducer. Lab Chart Pro Software Version 7 displayed the results of signal amplification achieved using Power Lab (4/25). Before delivering any drug, the exposed region was coated with a damp cotton swab and left to equilibrate for 15 ± 5 min. Standard one μg/kg dosages of acetylcholine and adrenaline were administered to induce hypotension and hypertension before testing.[93]

5.7.3. Isoproterenol-Induced Chronic Myocardial Infarction. The 21-day duration of the research was designed to induce MI. Normal saline was used to dissolve Fip.Cr and isoproterenol (ISO). Randomly dividing thirty-five rats weighing 120−170 g into seven groups and housing them in separate cages. Each group consists of five SD rats.

1st Group: The negative control (NC) group was orally administered 10 mL/kg bw of normal saline.

2nd Group: The intoxicated control (IC) group was administered a dosage of 5 mg/kg bw of ISO subcutaneously daily for 14 days (from the experiment's eighth day to its twenty-first day).

3rd Group: The group treated with standard (VRP) was administered a dosage of 10 mg/kg bw of verapamil orally daily for 21 days.

4th Group: The group treated with standard (CAR) was administered a dosage of 10 mg/kg bw of carvedilol orally daily for 21 days.

5th Group: The group treated with hydromethanolic extract (FLD) was administered a dosage of 100 mg/kg bw of Fip.Cr orally daily for 21 days.

6th Group: The group treated with hydromethanolic extract (FHD) was administered a dosage of 200 mg/kg bw of Fip.Cr orally daily for 21 days.

7th Group: The control group treated with hydromethanolic extract (FWI) was administered a dosage of 200 mg/kg bw of Fip.Cr orally daily for 21 days. This cohort was utilized to assess the effects of Fip.Cr without ISO on model parameter values.

After 1 h of pretreatment with verapamil, carvedilol, and Fip.Cr, subcutaneous injections of ISO (5 mg/kg) were administered for 14 consecutive days, beginning on the eighth day and ending on the twenty-first day, except for the seventh group, which did not receive ISO.[94]

Sample Collection

Twenty-four hours following their last injection of ISO, the rats were anesthetized with 40 mg/kg of intraperitoneal ketamine, and retro-orbital sinus blood was collected into coagulant and anticoagulant tubes containing EDTA to determine biochemical indicators. Serum and plasma were separated from blood samples by centrifuging them at 4 °C for 15 min at 4500 rpm. The blood samples were then frozen at −20 °C. The animals were euthanized via cervical dislocation, and cardiac tissue was extracted for research. For RT-PCR investigation, the cardiac tissues were immediately cleaned with ice-cold saline, immersed in trizole, and frozen. For histological studies, cardiac tissues are preserved in 10% formalin. Rat feces samples were collected and frozen for RT-PCR microbiota analysis.

5.7.3.1. Determination of Biometrical Indicators. Biometrical indicators such as left ventricular heart (LVH) weight and index (LVH weight/body weight ratio), heart weight, LVH thickness, tail and tibia lengths indices (heart weight/length ratio), heart index (heart weight/body weight ratio), and heart diameter were used to evaluate cardiac hypertrophy.[95]

5.7.3.2. Determination of Cardiac Serum Biochemical Indicators. Myocardial infarction indicators were evaluated using widely available enzymatic kits. These indicators consisted of creatine kinase MB (CK-MB), lipid profile, creatine phosphokinase (CPK), serum interleukin-6 (IL-6), troponin T (cTnT), aspartate transaminase (AST), arterial natriuretic

https://doi.org/10.1021/acsomega.3c07655
ACS Omega 2024, 9, 3642−3668

peptide (ANP), lactate dehydrogenase (LDH), and alanine transaminase (ALT).

5.7.3.3. qRT-PCR. qRT-PCR was used to examine the level of mRNA expression for ASC, NLRP3, caspase-1, TNF-α, IL-1β, and IL-6. According to the manufacturer's guidelines, the TRIzol reagent (USA, California, Carlsbad, Invitrogen) was used to isolate and purify total RNA from rat heart tissues after homogenization of frozen tissues. cDNA was subsequently synthesized from total RNA using an M-MLV reverse transcription enzyme kit using the manufacturer's instructions. RNA levels of ASC, NLRP3, caspase-1, TNF-α, IL-1β, and IL-6 were quantified by qPCR using SYBR-Green Supermix (USA, California, Hercules, Bio-Rad) after reverse transcription. The $2^{-\Delta\Delta Ct}$ technique was used to analyze the data. The housekeeping gene for the mRNA study was GAPDH. Table 9 displays the primer sequences.[96,97]

5.7.3.4. Microbiota Analysis. qRT-PCR was performed for microbiota analysis, including V2 (total bacterial load/hyperactive region), Firmicutes, and Lactobacillus in rat feces samples.

5.7.3.5. Histopathological Examinations. Following a xylene wash and paraffin fixation at 56 °C, a series of alcohol dilutions (70−100%) were used to dehydrate the hearts. Hematoxylin and eosin (H&E) stains were applied to deparaffinized and 4 μm thick heart slices. A microscope with 10× magnification was used to acquire digital photographs.

5.8. In Silico Investigations. *5.8.1. Drug-Likeness and ADMET.* *Fumaria indica* (Hausskn.) Pugsley hydro-methanolic extract bioactive components were investigated for drug-likeness indicators and ADMET (absorption, distribution, metabolism, excretion, and toxicity) using ADMETlab 2.0, Qikprop module Maestro (Schrodinger suite 2021), SWISS ADME (http://www.swiss-adme.ch/) retrieved on May 01, 2023, and admetSAR.[98]

5.8.2. Modeling Protein Homology. The three-dimensional structure of a protein is determined using homology modeling based on the sequence similarity between at least one PDB template and UniProt. This approach is predicated on the notion that the target protein's structural conformation is superior to its amino acid sequence in terms of stability. The ExPASy ProtParam (https://web.expasy.org/protparam) application was used to calculate numerous chemical and physical characteristics, accessed on June 2, 2023,[99] including projected isoelectric point, extinction coefficient, molecular weight, instability index, totally positive and negative charged residues, amino acid content, GRAVY, and aliphatic index.

We discovered templates utilizing UniProt sequences, searched for homology using BLAST (NCBI PDB Database), conducted sequence alignment using ClustW, and formulated a model, which was subsequently validated during homology modeling (Schrodinger suite 2021−3, Maestro 12.9). Ramachandran plots and Protein's Reliability Report found that the protein model did not meet the standards.

The building model was refined using the Prime refinement loop and Prime minimization module, with the VSGB solvation model and OPLS4 force field. On June 3, 2023, PROCHECK was executed on the minimized protein model Ramachandran plots using the Web site (https://saves.mbi.ucla.edu/) SAVES v6.0.[100,101]

5.8.3. Network Pharmacology Analysis. We utilized techniques Xiao et al.[102] had previously outlined for network pharmacology analysis.

Prospective Target Evaluation. The Swiss Target Prediction and Drugbank databases predicted the proteins most likely to be targeted by bioactive compounds. The probability-based cutoff value of 0.03 led to the selection of 307 targets.

The databases DisGeNET (https://www.disgenet.org/), Pubmed, and Gene card were leveraged on May 21, 2023, to identify disease targets containing the word "hypertension". The VarElect database (https://ve.genecards.org/), accessed on May 22, 2023, was used to construct genetic and phenotypic disease association scores for hypertension targets. The 150 top targets were saved for bioactive chemicals and illness target intersection analysis using Venny 2.1, a web-based toolbox retrieved on May 22, 2023: https://bioinfogp.cnb.csic.es/tools/venny/, and the relationship between the targets of bioactive substances and disease-associated proteins is depicted using a Venn diagram. ShinyGO version 0.77 was also used to enrich KEGG pathways and conduct Gene Ontology analysis on corelative targets. Pathway database of KEGG and GO biological process for top ten was conducted using "Human" and an FDR cutoff of 0.05. We categorized the pathway database by fold enrichment and chose using FDR.

Networks Construction. Cytoscape 3.9.1 would utilize the string to retrieve Protein−protein Interaction (PPI) for hypertension-related targets. We constructed the Compounds Targets Disease (CTD) and Compounds Targets Pathways (CTP) networks using Cytoscape 3.9.1.

Target Analysis and Pathways Evaluation. MCODE was implemented to detect clusters in PPI networks (densely connected regions). A separate list of putative FIP targets in the MCODE clusters for hypertensive illness was compiled. These common targets were considered potential hub proteins for FIP in hypertension treatment. GenomeNet was utilized to identify the components linked with these targets. Based on the KEGG pathways enrichment study results, pathways comprising the key proteins were discovered and considered.

5.8.4. Molecular Docking. Network pharmacology explores the affinity and stability of target proteins using functional chemicals or significant ligands. The two-dimensional ligand structures were retrieved from "PubChem" on June 4, 2023 (https://pubchem.ncbi.nih.gov) in format SDF and submitted to LigPrep ligand minimization, ionization, and optimization. Including the force field OPLS4 to optimize ligands and reduce energy enhanced the efficacy and precision of energy-optimized conformational predictions of protein−ligand. Using Epik to produce pH-appropriate (7.0 ± 2.0) ionization states for suspected protomers. Each ionized ligand was transformed into a tautomeric version, and the desalt's tool was utilized to retain the highest atomic counts of ligands. Each ligand under consideration had up to 10 stereoisomers made with the stereoizer while maintaining the acquired data on chiral stereogenesis.

Using the task protein preparation, we performed hydrogen bond assignment, het state minimization, optimization, and ionization of the resultant model protein's three-dimensional crystalline structures. Redundant binding sites were removed from the developed model protein structure to assess whether the ligand-protein interaction is multimeric or dimeric. The Chemical Components Dictionary database rearranged the unstructured amino acid residues and het groups. Alterations were made to the charges typically associated with metal ions and their neighboring atoms, and the number of covalent bonds between metal ions and adjoining atoms was reduced to zero. Disulfide connections are formed when protein sulfur atoms are less than 3.2 Å apart. The command prime validated and rectified structural defects in proteins, especially those resulting

https://doi.org/10.1021/acsomega.3c07655
ACS Omega 2024, 9, 3642−3668

from side-chain atom absences. Across a pH range of 7.4 ± 2.0, the group het protonation and metal/cofactor charge states were determined with an accuracy of 5.0 Å using the Epik tool. Within 5.0 Å of the protein structure, water molecules and het groups replaced hydrogen atoms. PROPKA application at a pH of 7.4 increased the hydrogen bond distribution throughout protein structures. Introducing the force field, OPLS4 decreased constraint energies and improved protein architectures.

The binding sites were determined via receptor grid generation. In part, improved ligand binding to protein pockets was achieved using a cube grid to predict coordinates based on bibliographic research and a module sitemap. VGCC used coordinates for PDB: 8EOI; x= 175.22, y = 203.5, z = 169.06. Under the partial charge threshold of 0.25 for proteins with nonpolar atomic van der Waals radius, the nonpolar regions' receptor potential is lowered by scaling factor 1.

Extra precision glide dock (XP) was linked with a previously prepared grid receptor file to facilitate the induced docking fitness of proteins and ligand precursors. The partial charge threshold and Radii van der Waals' scaling factor values were 0.15 and 0.80 Å, respectively. Adjustments have been made to the ligands sampling that facilitates flexible docking to create conformers by including ring conformations and nonring nitrogen inversions. In addition, the torsion sampling bias was implemented near a bond. The Epik indicates the accrual of docking score penalties.

We employed Prime MM-GBSA for Extra precision docking results, which computed the binding energies of ligands to protein structures utilizing the VSGB solvation model and OPLS4 force field (Schrodinger suite 2021−3, Maestro 12.9).[103]

Inhibition Constant.

$$\Delta G = -RT(\ln K_i)$$

T (cal mol^{-1} K^{-1}): 298 K ambient temperature; R: gas constant; ΔG: ligand's binding free energy.

$$K_i = e(-\Delta G/RT)$$

The above equations were used for the inhibition constant to calculate the ligand's binding free energy.

5.9. Statistical Analysis. The findings of the experiments were expressed as means ± SD. Logarithmic sigmoidal dose−response graphs were used to plot concentration−response curves. The EC_{50} (median effective concentration) with a 95% CI (confidence interval) was determined using sigmoidal dose−response graphs and a nonlinear regression curve fit. The *in vivo* results were evaluated using a one-way ANOVA followed by the Dunnett test with GraphPad Prism-9 to ascertain statistical significance. At the $p \leq 0.05$ level, there were significant findings.

■ ASSOCIATED CONTENT

Data Availability Statement

Data could be provided upon request from the corresponding author, Dr. Ambreen Aleem (Supervisor), ambreen.aleem@bzu.edu.pk.

Supporting Information

The Supporting Information is available free of charge at https://pubs.acs.org/doi/10.1021/acsomega.3c07655.

LC ESI-MS/MS spectra in negative and positive mode for tentative compounds of *Fumaria indica* (Hausskn.) Pugsley hydromethanolic extract; body weight gain percentage of individual rats by weeks: in acute toxicity study on (A) 7th day and (B) 14th day; in subacute toxicity study on (C) 7th day, (D) 14th day, (E) 21st day, and (F) 28th day; secondary structural sequence alignment of the 8EOI; top 150 pathogenic target genes related to hypertension analyzed via VarElect; most probable macromolecular targets of bioactive compounds; Venn diagram between compounds macromolecular targets and hypertension genes; top ten GO Biological process of bioactive compounds of *Fumaria indica* (Hausskn.) Pugsley hydromethanolic extract for hypertension-related target genes; top ten KEGG pathways of bioactive compounds of *Fumaria indica* (Hausskn.) Pugsley hydromethanolic extract for hypertension-related target genes; network analysis of hypertensive pathogenic target genes' interactions with phytoconstituents; network analysis of hypertensive pathogenic target genes' interactions with phytoconstituents and GO biological process (BP); network analysis of hypertensive pathogenic target genes' interactions with phytoconstituents and KEGG pathways; and interaction of Fip.Cr bioactive compounds and verapamil with CAC1C_ HUMAN (Q13936) (PDF)

■ AUTHOR INFORMATION

Corresponding Author

Ambreen Aleem − *Department of Pharmacology, Faculty of Pharmacy, Bahauddin Zakariya University, Multan 60800, Pakistan;* orcid.org/0000-0002-7722-2643; Phone: +923226100313; Email: ambreenaleem@hotmail.com, ambreen.aleem@bzu.edu.pk

Authors

Syed Adil Hussain Shah − *Department of Pharmacology, Faculty of Pharmacy, Bahauddin Zakariya University, Multan 60800, Pakistan*

Samia Latif Rana − *Department of Pharmacology, Faculty of Pharmacy, Bahauddin Zakariya University, Multan 60800, Pakistan*

Mohamed Mohany − *Department of Pharmacology and Toxicology, College of Pharmacy, King Saud University, Riyadh 11451, Saudi Arabia*

Marija Milošević − *Department of Biology and Ecology, Faculty of Science, University of Kragujevac, 34000 Kragujevac, Serbia*

Salim S. Al-Rejaie − *Department of Pharmacology and Toxicology, College of Pharmacy, King Saud University, Riyadh 11451, Saudi Arabia*

Muhammad Akmal Farooq − *Department of Pharmacy, University of Agriculture, Faisalabad 60800, Pakistan*

Muhammad Naeem Faisal − *Institute of Physiology and Pharmacology, University of Agriculture, Faisalabad 60800, Pakistan*

Complete contact information is available at: https://pubs.acs.org/10.1021/acsomega.3c07655

Author Contributions

Conceptualization: A.A., S.A.H.S.; Methodology; A.A., S.A.H.S., M.M., M.M., S.S.A.-R., S.L.R., M.A.F., M.N.F.; Resources; A.A., M.M., M.M., S.S.A.-R.; Data Analysis; A.A., S.A.H.S., M.M., M.M., S.S.A.-R.; Writing-original draft; S.A.H.S.

https://doi.org/10.1021/acsomega.3c07655
ACS Omega 2024, 9, 3642−3668

Author Contributions

S.A.H.S. performed all of the experiments as part of his Ph.D. research work under the supervision of Asst. Prof. Dr. Ambreen Aleem. S.A.H.S. wrote the manuscript draft. A.A. checked and corrected the draft and supervised the experimentators. S.L.R. assisted in the experimentation. M.A.F. and M.N.F. helped in performing qRT-PCR experiments. This work was funded by the Researchers Supporting Project (RSPD2023R758), King Saud University, Riyadh, Saudi Arabia. All data were generated in-house, and no paper mill was used. All authors agree to be accountable for all aspects of work, ensuring integrity and accuracy.

Funding

This work was funded by the Researchers Supporting Project (RSPD2023R758), King Saud University, Riyadh, Saudi Arabia.

Notes

The study was done with the agreement of the ethics committee of the Faculty of Pharmacy at Bahauddin Zakariya University in Multan, Pakistan (Letter no. EC/06-PhDL/S2018) and following international animal care standards.

The authors declare no competing financial interest.

■ ACKNOWLEDGMENTS

The authors appreciate the Researchers Supporting Project (RSPD2023R758), King Saud University, Riyadh, Saudi Arabia. The authors would like to thank the Physiology Department of the University of Agriculture in Faisalabad for providing the RT-PCR facility, as well as the pathologist Prof. Dr. Afra Samad of the Multan Medical and Dental College in Multan for their assistance.

■ ABBREVIATION

FIP: *Fumaria indica* (Hausskn.) Pugsley
Fip.Cr: *Fumaria indica* (Hausskn.) Pugsley hydromethanolic extract
BP: blood pressure
MI: myocardial infarction
PE: phenylephrine
TNF-α: tumor necrosis factor-alpha
MMGBSA: molecular mechanics energies combined surface area and generalized born
LogK_i: logarithmic of inhibition constant (K_i)

■ REFERENCES

(1) Roth, G. A.; Abate, D.; Abate, K. H.; Abay, S. M.; Abbafati, C.; Abbasi, N.; Abbastabar, H.; Abd-Allah, F.; Abdela, J.; Abdelalim, A.; Abdollahpour, I.; et al. Global, Regional, and National Age-Sex-Specific Mortality for 282 Causes of Death in 195 Countries and Territories, 1980−2017: A Systematic Analysis for the Global Burden of Disease Study 2017. *Lancet* **2018**, *392* (10159), 1736−1788.

(2) Kyu, H. H.; Abate, D.; Abate, K. H.; Abay, S. M.; Abbafati, C.; Abbasi, N.; Abbastabar, H.; Abd-Allah, F.; Abdela, J.; Abdelalim, A.; Abdollahpour, I.; et al. Global, Regional, and National Disability-Adjusted Life-Years (DALYs) for 359 Diseases and Injuries and Healthy Life Expectancy (HALE) for 195 Countries and Territories, 1990−2017: A Systematic Analysis for the Global Burden of Disease Study 2017. *Lancet* **2018**, *392* (10159), 1859−1922.

(3) Mensah, G. A.; Roth, G. A.; Fuster, V. The Global Burden of Cardiovascular Diseases and Risk Factors: 2020 and Beyond. *J. Am. Coll. Cardiol.* **2019**, *74*, 2529−2532.

(4) Sharifi-Rad, J.; Rodrigues, C. F.; Sharopov, F.; Docea, A. O.; Karaca, A. C.; Sharifi-Rad, M.; Karincaoglu, D. K.; Gülseren, G.; Şenol, E.; Demircan, E.; Taheri, Y.; Suleria, H. A. R.; Özçelik, B.; Kasapoğlu, K. N.; Gültekin-Özgüven, M.; Daşkaya-Dikmen, C.; Cho, W. C.; Martins, N.; Calina, D. Diet, Lifestyle and Cardiovascular Diseases: Linking Pathophysiology to Cardioprotective Effects of Natural Bioactive Compounds. *Int. J. Environ. Res. Public Health* **2020**, *17*, 2326.

(5) Ikeda, J. Eat for Life: The Food and Nutrition Board's Guide to Reducing Your Risk of Chronic Disease. *Am. J. Clin. Nutr.* **1993**, *57* (2), 233−234.

(6) Shahwan, A. J.; Abed, Y.; Desormais, I.; Magne, J.; Preux, P. M.; Aboyans, V.; Lacroix, P. Epidemiology of Coronary Artery Disease and Stroke and Associated Risk Factors in Gaza Community-Palestine. *PLoS One* **2019**, *14* (1), No. e0211131.

(7) Bansal, M. Cardiovascular Disease and COVID-19. *Diabetes Metab. Syndr. Clin. Res. Rev.* **2020**, *14* (3), 247−250.

(8) Mehra, M. R.; Desai, S. S.; Kuy, S.; Henry, T. D.; Patel, A. N. Cardiovascular Disease, Drug Therapy, and Mortality in Covid-19. *N. Engl. J. Med.* **2020**, *382* (25), No. e102.

(9) Current Medicine Group LLC 1 Kitt, J.; Fox, R.; Tucker, K. L.; McManus, R. J. New Approaches in Hypertension Management: A Review of Current and Developing Technologies and Their Potential Impact on Hypertension Care. *Curr. Hypertens. Rep.* **2019**, *21*, 44.

(10) Haldar, R. N. Global Brief on Hypertension: Silent Killer, Global Public Health Crisis. *Indian J. Phys. Med. Rehabil.* **2013**, *24* (1), 2−2.

(11) Thygesen, K.; Alpert, J. S.; Jaffe, A. S.; Chaitman, B. R.; Bax, J. J.; Morrow, D. A.; White, H. D.; Corbett, S.; Chettibi, M.; Hayrapetyan, H.; Roithinger, F. X.; Aliyev, F.; Sujayeva, V.; Claeys, M. J.; Smajić, E.; Kala, P.; Iversen, K. K.; El Hefny, E.; Marandi, T.; Porela, P.; Antov, S.; Gilard, M.; Blankenberg, S.; Davlouros, P.; Gudnason, T.; Alcalai, R.; Colivicchi, F.; Elezi, S.; Baitova, G.; Zakke, I.; Gustiene, O.; Beissel, J.; Dingli, P.; Grosu, A.; Damman, P.; Juliebo, V.; Legutko, J.; Morais, J.; Tatu-Chitoiu, G.; Yakovlev, A.; Zavatta, M.; Nedeljkovic, M.; Radsel, P.; Sionis, A.; Jemberg, T.; Müller, C.; Abid, L.; Abaci, A.; Parkhomenko, A. Fourth Universal Definition of Myocardial Infarction (2018). *Circulation* **2018**, *138* (20), e618−e651.

(12) Mendis, S.; Thygesen, K.; Kuulasmaa, K.; Giampaoli, S.; Mahonen, M.; Ngu Blackett, K.; Lisheng, L. World Health Organization Definition of Myocardial Infarction: 2008−09 Revision. *Int. J. Epidemiol.* **2011**, *40* (1), 139−146.

(13) Thygesen, K.; Alpert, J. S.; White, H. D. Universal Definition of Myocardial Infarction. *Circulation* **2007**, *116* (22), 2634−2653.

(14) Reed, G. W.; Rossi, J. E.; Cannon, C. P. Acute Myocardial Infarction. *Lancet* **2017**, *389*, 197−210.

(15) Nichols, M.; Townsend, N.; Scarborough, P.; Rayner, M. CardioPulse * Cardiovascular Disease in Europe 2014: Epidemiological Update * Heart Disease and Stroke Decline in Europe * Estimating an Individual Person's Course of Coronary Artery Calcification * The CardioScape Project * In Memoriam. *Eur. Heart J.* **2014**, *35* (42), 2929−2933.

(16) Neri, M.; Fineschi, V.; Paolo, M.; Pomara, C.; Riezzo, I.; Turillazzi, E.; Cerretani, D. Cardiac Oxidative Stress and Inflammatory Cytokines Response after Myocardial Infarction. *Curr. Vasc. Pharmacol.* **2015**, *13* (1), 26−36.

(17) Academic Press Sawyer, D. B.; Siwik, D. A.; Xiao, L.; Pimentel, D. R.; Singh, K.; Colucci, W. S. Role of Oxidative Stress in Myocardial Hypertrophy and Failure. *J. Mol. Cell. Cardiol.* **2002**, *34*, 379−388.

(18) Pasupathy, S.; Tavella, R.; Grover, S.; Raman, B.; Procter, N. E. K.; Du, Y. T.; Mahadavan, G.; Stafford, I.; Heresztyn, T.; Holmes, A.; Zeitz, C.; Arstall, M.; Selvanayagam, J.; Horowitz, J. D.; Beltrame, J. F. Early Use of N-Acetylcysteine With Nitrate Therapy in Patients Undergoing Primary Percutaneous Coronary Intervention for ST-Segment−Elevation Myocardial Infarction Reduces Myocardial Infarct Size (the NACIAM Trial [N-Acetylcysteine in Acute Myocardial Inf. *Circulation* **2017**, *136* (10), 894−903.

(19) Shaito, A.; Thuan, D. T. B.; Phu, H. T.; Nguyen, T. H. D.; Hasan, H.; Halabi, S.; Abdelhady, S.; Nasrallah, G. K.; Eid, A. H.; Pintus, G. Herbal Medicine for Cardiovascular Diseases: Efficacy, Mechanisms, and Safety. *Front. Pharmacol.* **2020**, *11*, 422.

(20) Patwardhan, B. Ethnopharmacology and Drug Discovery. *J. Ethnopharmacol.* **2005**, *100*, 50−52.

https://doi.org/10.1021/acsomega.3c07655
ACS Omega 2024, 9, 3642−3668

(21) Cordell, G. A.; Colvard, M. D. Some Thoughts on the Future of Ethnopharmacology *J. Ethnopharmacol.* 2005, *100*, 5−14, DOI: 10.1016/j.jep.2005.05.027.
(22) Leonti, M. The Relevance of Quantitative Ethnobotanical Indices for Ethnopharmacology and Ethnobotany. *J. Ethnopharmacol.* **2022**, *288*, No. 115008.
(23) Pirintsos, S.; Panagiotopoulos, A.; Bariotakis, M.; Daskalakis, V.; Lionis, C.; Sourvinos, G.; Karakasiliotis, I.; Kampa, M.; Castanas, E. From Traditional Ethnopharmacology to Modern Natural Drug Discovery: A Methodology Discussion and Specific Examples *Molecules* 2022, *27*, 4060, DOI: 10.3390/molecules27134060.
(24) Fabricant, D. S.; Farnsworth, N. R. The Value of Plants Used in Traditional Medicine for Drug Discovery. *Environ. Health Perspect.* **2001**, *109*, 69−75.
(25) Shah, S. M. A.; Akram, M.; Riaz, M.; Munir, N.; Rasool, G. Cardioprotective Potential of Plant-Derived Molecules: A Scientific and Medicinal Approach. *Dose-Response* **2019**, *17* (2), 155932581985224.
(26) Ahmad, L.; Semotiuk, A.; Liu, Q.; Rashid, W.; Mazari, P.; Rahim, K.; Sadia, S. Anti-Hypertensive Plants of Rural Pakistan:Current Use and Future Potential. *J. Complement. Med. Res.* **2018**, *7* (2), 138.
(27) Sajid, A.; Ahmad, T.; Ikram, M.; Khan, T.; Shah, A. J.; Mahnashi, M. H.; Alhasaniah, A. H.; Al Awadh, A. A.; Almazni, I. A.; Alshahrani, M. M. Cardioprotective Potential of Aqueous Extract of Fumaria Indica on Isoproterenol-Induced Myocardial Infarction in SD Rats. *Oxid. Med. Cell. Longev.* **2022**, *2022*, 1.
(28) Ahmad, L.; Semotiuk, A.; Zafar, M.; Ahmad, M.; Sultana, S.; Liu, Q. R.; Zada, M. P.; Abidin, S. Z. U.; Yaseen, G. Ethnopharmacological Documentation of Medicinal Plants Used for Hypertension among the Local Communities of DIR Lower. *Pakistan. J. Ethnopharmacol.* **2015**, *175*, 138−146.
(29) Guna, G. Pharmacological Activity of Fumaria Indica - A Review. *J. Phytopharm.* **2017**, *6* (6), 352. 2470−1343
(30) Rao, K. S.; Mishra, S. H. Hepatoprotective Activity of the Whole Plants of Fumaria Indica. *Indian J. Pharm. Sci.* **1997**, *59* (4), 165−170.
(31) Gilani, A. H.; Bashir, S.; Janbaz, K. H.; Khan, A. Pharmacological Basis for the Use of Fumaria Indica in Constipation and Diarrhea. *J. Ethnopharmacol.* **2005**, *96* (3), 585−589.
(32) Kumar, V.; Singh, G.; Rai, G.; Chatterjee, S. Effects of Ethanolic Extract of Fumaria Indica L. on Rat Cognitive Dysfunctions. *AYU (An Int. Q. J. Res. Ayurveda)* **2013**, *34* (4), 421.
(33) Shakya, A.; Soni, U. K.; Rai, G.; Chatterjee, S. S.; Kumar, V. Gastro-Protective and Anti-Stress Efficacies of Monomethyl Fumarate and a Fumaria Indica Extract in Chronically Stressed Rats. *Cell. Mol. Neurobiol.* **2016**, *36* (4), 621−635.
(34) Shakya, A.; Singh, G.; Chatterjee, S.; Kumar, V. Role of Fumaric Acid in Anti-Inflammatory and Analgesic Activities of a Fumaria Indica Extracts. *J. Intercult. Ethnopharmacol.* **2014**, *3* (4), 173.
(35) Hussain, T.; Siddiqui, H. H.; Fareed, S.; Vijayakumar, M.; Rao, C. V. Evaluation of Chemopreventive Effect of Fumaria Indica against N-Nitrosodiethylamine and CCl 4-Induced Hepatocellular Carcinoma in Wistar Rats. *Asian Pac. J. Trop. Med.* **2012**, *5* (8), 623−629.
(36) Qaddir, I.; Rasool, N.; Hussain, W.; Mahmood, S. Computer-Aided Analysis of Phytochemicals as Potential Dengue Virus Inhibitors Based on Molecular Docking, ADMET and DFT Studies. *J. Vector Borne Dis.* **2017**, *54* (3), 255−262.
(37) Fazal, H.; Ahmad, N.; Khan, M. A. Physico-Chemical, Phytochemical Evaluation and Dpph-Scavenging Antioxidant Potential in Medicinal Plants Used for Herbal Formulation in Pakistan. *Pak. J. Bot.* **2011**, *43*, 63−67.
(38) Razavi, R.; Kenari, R. E. Antioxidant Evaluation of Fumaria Parviflora L. Extract Loaded Nanocapsules Obtained by Green Extraction Methods in Oxidative Stability of Sunflower Oil. *J. Food Meas. Charact.* **2021**, *15* (3), 2448−2457.
(39) Păltinean, R.; Mocan, A.; Vlase, L.; Gheldiu, A. M.; Crişan, G.; Ielciu, I.; Voştinaru, O.; Crişan, O. Evaluation of Polyphenolic Content, Antioxidant and Diuretic Activities of Six Fumaria Species. *Molecules* **2017**, *22* (4), 639.
(40) Huang, Y. H.; Zhang, Z. Z.; Jiang, J. X. Relaxant Effects of Protopine on Smooth Muscles. *Acta Pharmacol. Sin.* **1991**, *12* (1), 16−19.
(41) Fahad, F. I.; Barua, N.; Shafiqul Islam, M.; Al Jawad Sayem, S.; Barua, K.; Uddin, M. J.; Nazim Uddin Chy, M.; Adnan, M.; Islam, M. N.; Sayeed, M. A.; Emran, T. Bin; Simal-Gandara, J.; Pagano, E.; Capasso, R. Investigation of the Pharmacological Properties of Lepidagathis Hyalina Nees through Experimental Approaches. *Life* **2021**, *11* (3), 180.
(42) Sinan, K. I.; Akpulat, U.; Aldahish, A. A.; Altunoglu, Y. C.; Baloğlu, M. C.; Zheleva-Dimitrova, D.; Gevrenova, R.; Lobine, D.; Mahomoodally, M. F.; Etienne, O. K.; Zengin, G.; Mahmud, S.; Capasso, R. LC-MS/HRMS Analysis, Anti-Cancer, Anti-Enzymatic and Anti-Oxidant Effects of Boerhavia Diffusa Extracts: A Potential Raw Material for Functional Applications. *Antioxidants* **2021**, *10* (12), 2003.
(43) Raza, M.; Al-Shabanah, O. A.; El-Hadiyah, T. M.; Al-Majed, A. A. Effect of Prolonged Vigabatrin Treatment on Hematological and Biochemical Parameters in Plasma, Liver and Kidney of Swiss Albino Mice. *Sci. Pharm.* **2002**, *70* (2), 135−145.
(44) Brice Landry, K.; Tariq, S.; Malik, A.; Sufyan, M.; Ashfaq, U. A.; Ijaz, B.; Shahid, A. A. Berberis Lyceum and Fumaria Indica: In Vitro Cytotoxicity, Antioxidant Activity, and in Silico Screening of Their Selected Phytochemicals as Novel Hepatitis C Virus Nonstructural Protein 5A Inhibitors. *J. Biomol. Struct. Dyn.* **2022**, *40* (17), 7829−7851.
(45) Gupta, P. C.; Sharma, N.; Rao, C. V. A Review on Ethnobotany, Phytochemistry and Pharmacology of Fumaria Indica (Fumitory). *Asian Pac. J. Trop. Biomed.* **2012**, *2* (8), 665−669.
(46) Gupta, P. C.; Rao, C. V. Morpho-Anatomical and Physicochemical Studies of Fumaria Indica (Hausskn.) Pugsley. *Asian Pac J. Trop. Biomed.* **2012**, *2* (10), 830−834.
(47) Pérez-Vizcaíno, F.; Cogolludo, A. L.; Villamor, E.; Tamargo, J. Role of K+ Channel Opening and Stimulation of Cyclic GMP in the Vasorelaxant Effects of Nicorandil in Isolated Piglet Pulmonary and Mesenteric Arteries: Relative Efficacy and Interactions between Both Pathways. *Br. J. Pharmacol.* **1998**, *123* (5), 847−854.
(48) Mehmood, M. H.; Anila, N.; Begum, S.; Syed, S. A.; Siddiqui, B. S.; Gilani, A. H. Pharmacological Basis for the Medicinal Use of Carissa Carandas in Constipation and Diarrhea. *J. Ethnopharmacol.* **2014**, *153* (2), 359−367.
(49) Li, W.; Altura, B. T.; Altura, B. M. Differential Effects of Methanol on Rat Aortic Smooth Muscle. *Alcohol* **1998**, *16* (3), 221−229.
(50) Saqib, F.; Wahid, M.; AL-Huqail, A. A.; Ahmedah, H. T.; Bigiu, N.; Irimie, M.; Moga, M.; Marc Vlaic, R. A.; Pop, O. L.; Chicea, L. M. Metabolomics Based Mechanistic Insights to Vasorelaxant and Cardioprotective Effect of Ethanolic Extract of Citrullus Lanatus (Thunb.) Matsum. & Nakai. Seeds in Isoproterenol Induced Myocardial Infraction. *Phytomedicine* **2022**, *100*, No. 154069.
(51) Saqib, F.; Janbaz, K. H. Rationalizing Ethnopharmacological Uses of Alternanthera Sessilis: A Folk Medicinal Plant of Pakistan to Manage Diarrhea, Asthma and Hypertension. *J. Ethnopharmacol.* **2016**, *182*, 110−121.
(52) Constantine, A.; Dimopoulos, K. Physiology of the Normal Heart. *Medicine (Baltimore)*. **2022**, *50* (6), 322−326.
(53) Neergheen-Bhujun, V. S. Underestimating the Toxicological Challenges Associated with the Use of Herbal Medicinal Products in Developing Countries. *Biomed Res. Int.* **2013**, *2013*, 1−9.
(54) Yuet Ping, K.; Darah, I.; Chen, Y.; Sreeramanan, S.; Sasidharan, S. Acute and Subchronic Toxicity Study of Euphorbia Hirta L. Methanol Extract in Rats. *Biomed Res. Int.* **2013**, *2013*, 1−14.
(55) Ukwuani, A. N.; Abubakar, M.; Hassan, S. W.; Agaie, B. M. Toxicological Studies of Hydromethanolic Leaves Extract of Grewia Crenata. *Int. J. Pharm. Sci. Drug Res.* **2012**, *4* (4), 245−249.
(56) Ezeja, M. I.; Anaga, A. O.; Asuzu, I. U. Acute and Sub-Chronic Toxicity Profile of Methanol Leaf Extract of Gouania Longipetala in Rats. *J. Ethnopharmacol.* **2014**, *151* (3), 1155−1164.
(57) Mukinda, J. T.; Syce, J. A. Acute and Chronic Toxicity of the Aqueous Extract of Artemisia Afra in Rodents. *J. Ethnopharmacol.* **2007**, *112* (1), 138−144.

(58) Jorum, O. H.; Piero, N. M. Haematological Effects of Dichloromethane-Methanolic Leaf Extracts of Carissa Edulis (Forssk.) Vahl in Normal Rat Models. *J. Hematol. Thromboembolic Dis.* **2016**, *04* (01), No. 1000232.
(59) Lawal, B.; Shittu, O. K.; Oibiokpa, F. I.; Mohammed, H.; Umar, S. I.; Haruna, G. M. Antimicrobial Evaluation, Acute and Sub-Acute Toxicity Studies of Allium Sativum. *J. Acute Dis.* **2016**, *5* (4), 296−301.
(60) Suganthy, N.; Muniasamy, S.; Archunan, G. Safety Assessment of Methanolic Extract of Terminalia Chebula Fruit, Terminalia Arjuna Bark and Its Bioactive Constituent 7-Methyl Gallic Acid: In Vitro and in Vivo Studies. *Regul. Toxicol. Pharmacol.* **2018**, *92*, 347−357.
(61) Zhang, Q.; Mao, Z.; Zhang, Q.; Qiu, J.; Jia, Z.; Qin, L. Acute and Sub-Chronic Toxicological Studies of the Iridoid Glycosides Extract of Lamiophlomis Rotata (Benth.) Kudo in Rats. *Regul. Toxicol. Pharmacol.* **2018**, *92*, 315−323.
(62) EL Moussaoui, A.; Bourhia, M.; Jawhari, F. Z.; Mechchate, H.; Slighoua, M.; Bari, A.; Ullah, R.; Mahmood, H. M.; Ali, S. S.; Ibenmoussa, S.; Bousta, D.; Bari, A. Phytochemical Identification, Acute, and Sub-Acute Oral Toxicity Studies of the Foliar Extract of Withania Frutescens. *Molecules* **2020**, *25* (19), 4528.
(63) Karthikeyan, K.; Bai, B. R. S.; Devaraj, S. N. Cardioprotective Effect of Grape Seed Proanthocyanidins on Isoproterenol-Induced Myocardial Injury in Rats. *Int. J. Cardiol.* **2007**, *115* (3), 326−333.
(64) Abbas, A. M. Cardioprotective Effect of Resveratrol Analogue Isorhapontigenin versus Omega-3 Fatty Acids in Isoproterenol-Induced Myocardial Infarction in Rats. *J. Physiol. Biochem.* **2016**, *72* (3), 469−484.
(65) Geng, Z.-H.; Huang, L.; Song, M.-B.; Song, Y.-M. Protective Effect of a Polysaccharide from Salvia Miltiorrhiza on Isoproterenol (ISO)-Induced Myocardial Injury in Rats. *Carbohydr. Polym.* **2015**, *132*, 638−642.
(66) Li, H.; Xie, Y.-H.; Yang, Q.; Wang, S.-W.; Zhang, B.-L.; Wang, J.-B.; Cao, W.; Bi, L.-L.; Sun, J.-Y.; Miao, S.; Hu, J.; Zhou, X.-X.; Qiu, P.-C. Cardioprotective Effect of Paeonol and Danshensu Combination on Isoproterenol-Induced Myocardial Injury in Rats. *PLoS One* **2012**, *7* (11), No. e48872.
(67) Abderrazak, A.; Syrovets, T.; Couchie, D.; El Hadri, K.; Friguet, B.; Simmet, T.; Rouis, M. NLRP3 Inflammasome: From a Danger Signal Sensor to a Regulatory Node of Oxidative Stress and Inflammatory Diseases. *Redox Biol.* **2015**, *4*, 296−307.
(68) Sandanger, Ø.; Ranheim, T.; Vinge, L. E.; Bliksøen, M.; Alfsnes, K.; Finsen, A. V.; Dahl, C. P.; Askevold, E. T.; Florholmen, G.; Christensen, G.; Fitzgerald, K. A.; Lien, E.; Valen, G.; Espevik, T.; Aukrust, P.; Yndestad, A. The NLRP3 Inflammasome Is Up-Regulated in Cardiac Fibroblasts and Mediates Myocardial Ischaemia-Reperfusion Injury. *Cardiovasc. Res.* **2013**, *99* (1), 164−174.
(69) Altaf, A.; Qu, P.; Zhao, Y.; Wang, H.; Lou, D.; Niu, N. NLRP3 Inflammasome in Peripheral Blood Monocytes of Acute Coronary Syndrome Patients and Its Relationship with Statins. *Coron. Artery Dis.* **2015**, *26* (5), 409−421.
(70) Liu, Y.; Lian, K.; Zhang, L.; Wang, R.; Yi, F.; Gao, C.; Xin, C.; Zhu, D.; Li, Y.; Yan, W.; Xiong, L.; Gao, E.; Wang, H.; Tao, L. TXNIP Mediates NLRP3 Inflammasome Activation in Cardiac Microvascular Endothelial Cells as a Novel Mechanism in Myocardial Ischemia/Reperfusion Injury. *Basic Res. Cardiol.* **2014**, *109* (5), 1−14.
(71) Tian, M.; Yuan, Y.; Li, J.; Gionfriddo, M. R.; Huang, R. Tumor Necrosis Factor-α and Its Role as a Mediator in Myocardial Infarction: A Brief Review. *Chronic Dis. Transl. Med.* **2015**, *1* (1), 18−26.
(72) Gerdes, V.; Gueimonde, M.; Pajunen, L.; Nieuwdorp, M.; Laitinen, K. How Strong Is the Evidence That Gut Microbiota Composition Can Be Influenced by Lifestyle Interventions in a Cardio-Protective Way? *Atherosclerosis* **2020**, *311*, 124−142.
(73) Han, Y.; Gong, Z.; Sun, G.; Xu, J.; Qi, C.; Sun, W.; Jiang, H.; Cao, P.; Ju, H. Dysbiosis of Gut Microbiota in Patients With Acute Myocardial Infarction. *Front. Microbiol.* **2021**, *12*, No. 680101.
(74) Cai, J. J.; Liu, Y.; Wang, J.; Wang, J. X.; Wang, Y.; Xu, S. B.; Cui, Z.; Gao, J. Lactobacillus Levels and Prognosis of Patients with Acute Myocardial Infarction. *J. Geriatr. Cardiol.* **2022**, *19* (2), 101−114.
(75) Heinrich, M.; Mah, J.; Amirkia, V. Alkaloids Used as Medicines: Structural Phytochemistry Meets Biodiversity—An Update and Forward Look *Molecules* 2021, *26*, 1836, DOI: 10.3390/molecules26071836.
(76) Hopkins, A. L. Network Pharmacology *Nat. Biotechnol.* 2007, *25*, 1110−1111, DOI: 10.1038/nbt1007-1110.
(77) Zhang, G. B.; Li, Q. Y.; Chen, Q. L.; Su, S. B. Network Pharmacology: A New Approach for Chinese Herbal Medicine Research. *Evidence-based Complementary and Alternative Medicine.* **2013**, *2013*, 1.
(78) Park, M.; Park, S. Y.; Lee, H. J.; Kim, C. E. A Systems-Level Analysis of Mechanisms of Platycodon Grandiflorum Based on a Network Pharmacological Approach *Molecules* 2018, *23*, 2841, DOI: 10.3390/molecules23112841.
(79) Stanzione, F.; Giangreco, I.; Cole, J. C. Use of Molecular Docking Computational Tools in Drug Discovery. In *Progress in Medicinal Chemistry*; Elsevier, 2021; Vol. *60*, pp 273−343.
(80) Qamar, M.; Akhtar, S.; Ismail, T.; Yuan, Y.; Ahmad, N.; Tawab, A.; Ismail, A.; Barnard, R. T.; Cooper, M. A.; Blaskovich, M. A. T.; Ziora, Z. M. Syzygium Cumini(L.),Skeels Fruit Extracts: In Vitro and in Vivo Anti-Inflammatory Properties. *J. Ethnopharmacol.* **2021**, *271*, No. 113805.
(81) Ganzera, M.; Sturm, S. Recent Advances on HPLC/MS in Medicinal Plant Analysis—An Update Covering 2011−2016. *J. Pharm. Biomed. Anal.* **2018**, *147*, 211−233.
(82) Hussain Shah, S. A.; Aleem, A. Investigations of Plausible Pharmacodynamics Supporting the Antispasmodic, Bronchodilator, and Antidiarrheal Activities of Berberis Lycium Royle. Via in Silico, in Vitro, and in Vivo Studies. *J. Ethnopharmacol.* **2023**, *305*, No. 116115.
(83) Rowan, A. N. Guide for the Care and Use of Laboratory Animals. *J. Med. Primatol.* **2017**, *8* (2), 128−128.
(84) Saqib, F.; Wahid, M.; AL-Huqail, A. A.; Ahmedah, H. T.; Bigiu, N.; Irimie, M.; Moga, M.; Marc Vlaic, R. A.; Pop, O. L.; Chicea, L. M. Metabolomics Based Mechanistic Insights to Vasorelaxant and Cardioprotective Effect of Ethanolic Extract of Citrullus Lanatus (Thunb.) Matsum. & Nakai. Seeds in Isoproterenol Induced Myocardial Infraction. *Phytomedicine* **2022**, *100*, No. 154069.
(85) Saqib, F.; Janbaz, K. H. Rationalizing Ethnopharmacological Uses of Alternanthera Sessilis: A Folk Medicinal Plant of Pakistan to Manage Diarrheam Asthma and Hypertension. *J. Ethnopharmacol.* **2016**, *182*, 110−121.
(86) Gilani, A. H.; Khan, A.; Raoof, M.; Ghayur, M. N.; Siddiqui, B. S.; Vohra, W.; Begum, S. Gastrointestinal, Selective Airways and Urinary Bladder Relaxant Effects of Hyoscyamus Niger Are Mediated through Dual Blockade of Muscarinic Receptors and Ca 2+ Channels. *Fundam. Clin. Pharmacol.* **2008**, *22* (1), 87−99.
(87) Kamkaew, N.; Scholfield, C. N.; Ingkaninan, K.; Maneesai, P.; Parkington, H. C.; Tare, M.; Chootip, K. Bacopa Monnieri and Its Constituents Is Hypotensive in Anaesthetized Rats and Vasodilator in Various Artery Types. *J. Ethnopharmacol.* **2011**, *137* (1), 790−795.
(88) Ghosh, D.; Mondal, S.; Ramakrishna, K. Acute and Sub-Acute (30-Day) Toxicity Studies of Aegialitis Rotundifolia Roxb., Leaves Extract in Wistar Rats: Safety Assessment of a Rare Mangrove Traditionally Utilized as Pain Antidote. *Clin. Phytoscience* **2019**, *5* (1), 13.
(89) OECD/OECDE. *Test No. 407: Repeated Dose 28-Day Oral Toxicity Study in Rodents; OECD Guidelines for the Testing of Chemicals, Section 4*; OECD, 2008.
(90) Ugwah-Oguejiofor, C. J.; Okoli, C. O.; Ugwah, M. O.; Umaru, M. L.; Ogbulie, C. S.; Mshelia, H. E.; Umar, M.; Njan, A. A. Acute and Sub-Acute Toxicity of Aqueous Extract of Aerial Parts of Caralluma Dalzielii N E. Brown in Mice and Rats. *Heliyon* **2019**, *5* (1), No. e01179.
(91) EL Moussaoui, A.; Bourhia, M.; Jawhari, F. Z.; Mechchate, H.; Slighoua, M.; Bari, A.; Ullah, R.; Mahmood, H. M.; Ali, S. S.; Ibenmoussa, S.; Bousta, D.; Bari, A. Phytochemical Identification, Acute, and Sub-Acute Oral Toxicity Studies of the Foliar Extract of Withania Frutescens. *Molecules* **2020**, *25* (19), 4528.
(92) Chebaibi, M.; Bousta, D.; Chbani, L.; Ez zoubi, Y.; Touiti, N.; Achour, S. Acute Toxicity of Plants Mixture Used in Traditional

Treatment of Edema and Colic Renal in Morocco. *Sci. Afr.* **2019**, *6*, No. e00152.
(93) Saqib, F.; Janbaz, K. H. Ethnopharmacological Basis for Folkloric Claims of Anagallis Arvensis Linn. (Scarlet Pimpernel) as Prokinetic, Spasmolytic and Hypotensive in Province of Punjab, Pakistan. *J. Ethnopharmacol.* **2021**, *267*, No. 113634.
(94) Eladwy, R. A.; Mantawy, E. M.; El-Bakly, W. M.; Fares, M.; Ramadan, L. A.; Azab, S. S. Mechanistic Insights to the Cardioprotective Effect of Blueberry Nutraceutical Extract in Isoprenaline-Induced Cardiac Hypertrophy. *Phytomedicine* **2018**, *51*, 84−93.
(95) Elasoru, S. E.; Rhana, P.; de Oliveira Barreto, T.; Naves de Souza, D. L.; Menezes-Filho, J. E. R.; Souza, D. S.; Loes Moreira, M. V.; Gomes Campos, M. T.; Adedosu, O. T.; Roman-Campos, D.; Melo, M. M.; Cruz, J. S. Andrographolide Protects against Isoproterenol-Induced Myocardial Infarction in Rats through Inhibition of L-Type Ca2+ and Increase of Cardiac Transient Outward K+ Currents. *Eur. J. Pharmacol.* **2021**, *906*, No. 174194.
(96) Zaafan, M. A.; Abdelhamid, A. M. The Cardioprotective Effect of Astaxanthin against Isoprenaline-Induced Myocardial Injury in Rats: Involvement of TLR4/NF-KB Signaling Pathway. *Eur. Rev. Med. Pharmacol. Sci.* **2021**, *25* (11), 4099−4105.
(97) Yu, Y.; Jin, L.; Zhuang, Y.; Hu, Y.; Cang, J.; Guo, K. Cardioprotective Effect of Rosuvastatin against Isoproterenol-Induced Myocardial Infarction Injury in Rats. *Int. J. Mol. Med.* **2018**, *41* (6), 3509−3516.
(98) Gajjar, N. D.; Dhameliya, T. M.; Shah, G. B. In Search of RdRp and Mpro Inhibitors against SARS CoV-2: Molecular Docking, Molecular Dynamic Simulations and ADMET Analysis. *J. Mol. Struct.* **2021**, *1239*, No. 130488.
(99) Chauhan, V.; Singh, M. P. Immuno-Informatics Approach to Design a Multi-Epitope Vaccine to Combat Cytomegalovirus Infection. *Eur. J. Pharm. Sci.* **2020**, *147*, No. 105279.
(100) Yu, Z.; Kang, L.; Zhao, W.; Wu, S.; Ding, L.; Zheng, F.; Liu, J.; Li, J. Identification of Novel Umami Peptides from Myosin via Homology Modeling and Molecular Docking. *Food Chem.* **2021**, *344*, No. 128728.
(101) Subhani, S.; Jayaraman, A.; Jamil, K. Homology Modelling and Molecular Docking of MDR1 with Chemotherapeutic Agents in Non-Small Cell Lung Cancer. *Biomed. Pharmacother.* **2015**, *71*, 37−45.
(102) Xiao, P.-T; Liu, S.-Y; Kuang, Y.-J; Jiang, Z.-M; Lin, Y.; Xie, Z.-S.; Liu, E. H. Network Pharmacology Analysis and Experimental Validation to Explore the Mechanism of Sea Buckthorn Flavonoids on Hyperlipidemia. *J. Ethnopharmacol.* **2021**, *264*, No. 113380.
(103) Sirous, H.; Chemi, G.; Campiani, G.; Brogi, S. An Integrated in Silico Screening Strategy for Identifying Promising Disruptors of P53-MDM2 Interaction. *Comput. Biol. Chem.* **2019**, *83*, No. 107105.

https://doi.org/10.1021/acsomega.3c07655
ACS Omega 2024, 9, 3642−3668